1-1-2015

# Brain Injury Induced Prefrontal Cortex Circuit Dysfunction Contributes to Working Memory Impairment

Colin Smith
*University of Pennsylvania*, colinsmith414@gmail.com

# Brain Injury Induced Prefrontal Cortex Circuit Dysfunction Contributes to Working Memory Impairment

**Abstract**
Traumatic Brain Injury (TBI) is the most common cause of brain damage resulting in disability, both in the United States and worldwide. TBI patients suffer from profound impairments in memory function. Lateral fluid percussion injury (LFPI) is the most common animal model of TBI and recreates the memory symptoms experienced by TBI survivors. Using a combination of behavioral testing and neurophysiological recording I investigated dysfunction in the brain circuits underlying post-TBI memory impairment in LFPI animals. I demonstrated that LFPI animals suffer from sustained working memory impairment in the first week after brain injury. Additionally, I determined the neurophysiological changes to the medial prefrontal cortex, a key component of the circuitry underlying working memory. The medial prefrontal cortex displays layer-specific changes to synaptic transmission and intrinsic excitability as well as decreased network excitability after brain injury. This pattern of physiological changes is similar to post-TBI alterations in the hippocampus, another key structure underlying post-TBI memory impairment. Despite the relative lack of attention paid to the medial prefrontal cortex by the TBI field, functional changes in the medial prefrontal cortex after TBI are likely a post-TBI substrate of working memory impairment.

**Degree Type**
Dissertation

**Degree Name**
Doctor of Philosophy (PhD)

**Graduate Group**
Neuroscience

**First Advisor**
Akiva S. Cohen

**Keywords**
Electrophysiology, Prefrontal Cortex, Traumatic Brain Injury, Working Memory

**Subject Categories**
Neuroscience and Neurobiology

# BRAIN INJURY INDUCED PREFRONTAL CORTEX CIRCUIT DYSFUNCTION CONTRIBUTES TO WORKING MEMORY IMPAIRMENT

Colin J. Smith

A DISSERTATION

in

Neuroscience

Presented to the Faculties of the University of Pennsylvania

in

Partial Fulfillment of the Requirements for the

Degree of Doctor of Philosophy

2015

Supervisor of Dissertation

___

Dr. Akiva S. Cohen, Research Associate Professor of Critical Care Medicine

Graduate Group Chairperson

_____

Dr. Joshua I. Gold, Professor of Neuroscience

Dissertation Committee

Dr. Minghong Ma, Associate Professor of Neuroscience

Dr. David F. Meaney, Solomon R. Pollack Professor of Bioengineering

Dr. Michael J. Kahana, Professor of Psychology

Dr. Leslie S. Satin, Professor of Pharmacology, University of Michigan Medical School

BRAIN INJURY INDUCED PREFRONTAL CORTEX CIRCUIT DYSFUNCTION CONTRIBUTES

TO WORKING MEMORY IMPAIRMENT

To my mother, father, Nana, and Bup. Thank you for making this all possible.

## ACKNOWLEDGMENT

I'd like to first and foremost acknowledge everyone in the Cohen laboratory who has played a vital role in my education and the work presented here. I would have learned and produced very little but for the outstanding support of my fellow lab members. Specifically, Dr. Sheriff Brian Johnson and Dr. Guoxiang Xiong who have both provided amazing guidance and support since my first day in the lab. Additionally, I would be nowhere without an outstanding cast of technicians who provided both support and lent their surgical skills to my work, including Jackie Elkind, Brendan Putnam, Christian Cruz and Hannah Matheny.

Furthermore, I have received support and friendship from the rest of the students in the neuroscience graduate group. This close knit community was one of the reasons I chose to pursue my PhD at Penn, and the support I have received has never wavered and for that I'll always be thankful. I'd especially like to thank Chris Palmer, with whom it's been a great joy to share a lab, desk, and more than a few drinks with for the past four years.

I cannot overstate the importance of the role of my mentor, Akiva S. Cohen, in my graduate work. Very early in my time in the lab he made it clear that he would allow me the freedom to pursue whatever project(s) I could dream up. This has made all the difference to me, keeping me motivated, enthusiastic and invested when I might otherwise have become disillusioned in the face of struggles. Not only did Dr. Cohen allow me scientific freedom, but also the freedom to pursue other avenues and career paths outside of the normal academic track. For this I am eternally grateful.

Finally, I'd like to acknowledge the people in my life who have supported me outside the laboratory. Friends and family have played a unique role in this project, keeping me focused on what's important and helping me through the tougher times. I'd especially like to acknowledge my wonderful wife Carrie. With her constantly positive attitude, she has done the lion's share of dealing with my frustrations and keeping me on track. I'd be lost without her.

# ABSTRACT

BRAIN INJURY INDUCED PREFRONTAL CORTEX CIRCUIT DYSFUNCTION CONTRIBUTES TO WORKING MEMORY IMPAIRMENT

Colin J. Smith

Akiva S. Cohen, PhD

Traumatic Brain Injury (TBI) is the most common cause of brain damage resulting in disability, both in the United States and worldwide. TBI patients suffer from profound impairments in memory function. Lateral fluid percussion injury (LFPI) is the most common animal model of TBI and recreates the memory symptoms experienced by TBI survivors. Using a combination of behavioral testing and neurophysiological recording I investigated dysfunction in the brain circuits underlying post-TBI memory impairment in LFPI animals. I demonstrated that LFPI animals suffer from sustained working memory impairment in the first week after brain injury. Additionally, I determined the neurophysiological changes to the medial prefrontal cortex, a key component of the circuitry underlying working memory. The medial prefrontal cortex displays layer-specific changes to synaptic transmission and intrinsic excitability as well as decreased network excitability after brain injury. This pattern of physiological changes is similar to post-TBI alterations in the hippocampus, another key structure underlying post-TBI memory impairment. Despite the relative lack of attention paid to the medial prefrontal cortex by the TBI field, functional changes in the medial prefrontal cortex after TBI are likely a post-TBI substrate of working memory impairment.

TABLE OF CONTENTS

LIST OF TABLES

**LOCAL FIELD POTENTIAL RECORDINGS IN AWAKE-BEHAVING ANIMALS: PILOT EXPERIMENTS AND METHOD DEVELOPMENT**

LIST OF FIGURES

**BRAIN INJURY IMPAIRS WORKING MEMORY AND PREFRONTAL CIRCUIT FUNCTION**



**LOCAL FIELD POTENTIAL RECORDINGS IN AWAKE-BEHAVING ANIMALS: PILOT EXPERIMENTS AND METHOD DEVELOPMENT**

# INTRODUCTION

More than 1.5 million people in the United States suffer a Traumatic Brain Injury (TBI) each year (Rutland-Brown et al., 2006). TBI is the most common cause of brain damage resulting in disability, both in the United States and worldwide (Rassovsky et al., 2015). Improvements in medical care have increased the number of survivors of TBI, however many of these individuals suffer from long-term disabilities that greatly reduce their quality of life (Zaloshnja et al., 2008). TBI predominantly causes damage to the frontal and temporal lobes of the cerebral cortex, and this damage causes severe neuropsychological sequelae, including persistent deficits to working memory, that disrupt the lives of TBI survivors (McAllister, 1992; McAllister et al., 2006; Riggio, 2010; Stuss, 2011; Palacios et al., 2012). Diminished activity of frontal lobe structures has been causally implicated as underlying working memory deficits following TBI (Sánchez-Carrión et al., 2008) and specific damage to the frontal lobes in brain-injured patients has been associated with difficulty maintaining performance in the workplace (Stuss, 2003). The most common type of brain injury is mild traumatic brain injury (mTBI), a term synonymous with concussion, and accounts for roughly 80% of TBI cases worldwide (Faul and Coronado, 2015).

Mild TBI can lead to an array of long-lasting neurological impairments (Laker, 2011). While the difference between mild and moderate to severe TBI is not well established and often debated due to the heterogeneous nature of physical injury, the American Congress of Rehabilitation Medicine delineates mTBI as “a traumatically induced physiologic disruption of brain function including: (1) any period of loss of

consciousness; (2) any loss of memory for events immediately before or after the accident; (3) any alteration in mental state at the time of the accident (eg, feeling dazed, disoriented, or confused); and (4) focal neurological deficits that may or may not be transient". However to remain in the mTBI categorization patients must not lose consciousness for more than 30 minutes, have a Glasglow Coma Scale score below 13, or have post-traumatic amnesia for greater than 24 hours (ACOR Medicine, 1993). The persistent cognitive difficulties experienced after mTBI, including working memory impairment, are often referred to as post-concussion syndrome (McHugh et al., 2006). The symptoms of post-concussion syndrome vary by individual but most often include difficulties with memory and attention (Stuss et al., 1985; McHugh et al., 2006), cognitive abilities that are well known to depend on contributions of the temporal and frontal lobes (Lishman, 1968; Kovner and Stamm, 1972; Olton et al., 1988; Uhl et al., 1990; Markowitsch et al., 1993).

Despite the pervasiveness of TBI, there is currently no accepted therapy to restore deficits in cognitive ability suffered by TBI survivors. Post-injury care is palliative, behavioral rehabilitation success is limited, and no treatment strategies exist that target the underlying causes of the cognitive and memory deficits that affect the lives of TBI patients. However, there is a demonstrated interest in developing targeted therapies with hundreds of clinical trials currently enrolling TBI patients for a variety of types of trials, in an effort to ease the suffering brought on by this life-changing injury.

To model TBI in rodent systems amenable to invasive experimental manipulations,

researchers developed an experimental model of brain injury known as lateral fluid percussion injury (LFPI). LFPI was developed for the rat in the late 1980s, and based off of a previous fluid percussion injury model which used larger animals (Lewelt et al., 1982; McIntosh et al., 1987; 1989; Lewelt et al., 2009). Roughly ten years after fluid percussion was established in the rat, it was adapted for use in mouse (Carbonell et al., 1998). Using LFPI to model human brain injury quickly grew in popularity as evidenced by the fact that LFPI is currently the most common animal model of experimental traumatic brain injury (Thompson et al., 2005). The LFPI procedure provides a consistent injury that reproduces many key features of human TBI including neuronal cell loss, gliosis, ionic perturbation and memory deficits (Dixon et al., 1987; McIntosh et al., 1987; 1989; Lyeth et al., 1990; Smith et al., 1991; Gorman et al., 1993; Witgen et al., 2005; Schwarzbach et al., 2006; Bonislawski et al., 2007). LFPI produces an injury that has both focal and diffuse components, and despite subtle differences has largely been replicated across laboratories (Thompson et al., 2005). The LFPI model allows for a range of severities of experimental TBI including a mild to moderate injury that does not cause rupturing of the dura mater, the thick membrane that is the outermost layer of the meninges. This provides an advantage over models of brain injury that cause dural breaches and bleeding that are generally not components of human mTBI.

Animal models of mTBI cause regionally specific disruptions in the balance between excitatory and inhibitory synaptic transmission (henceforth, E/I balance) in the hippocampus (Toth et al., 1997; D'Ambrosio et al., 1998; Witgen et al., 2005). Specifically, the dentate gyrus is more excitable after injury while hippocampal area CA1 is less excitable after injury (Witgen et al., 2005). The regional specificity and bi-directionality of the shifts in excitability within disrupted memory circuits have lead

researchers to conceptualize mTBI as a neurological disease with a basis in malfunctioning circuit components.

Within the hippocampus, research has sought to understand the basis for the shifts in E/I balance in terms of excitatory and inhibitory synaptic transmission, as well as specific types of cells that may be preferentially affected by injury. In particular, previous research has identified mossy cells, an excitatory interneuron type within the dentate gyrus, as a source of enhanced excitatory synaptic drive after injury contributing to post-injury hyperexcitability (Santhakumar et al., 2000). Similarly, augmented inhibitory drive provided by local inhibitory neurons in stratum radiatum of area CA1 has been shown to contribute to the network hypoexcitability observed after mTBI (Johnson et al., 2014). Studies of physiological alterations have not been limited to synaptic physiology however, with the contributions of ion pumps (Ross and Soltesz, 2000; Bonislawski et al., 2007) and intrinsic excitability (Howard et al., 2007) also hypothesized to play a role in post-TBI hippocampal circuit alterations.

While the underlying reasons for preferential alteration of certain cell types (and thus circuit components) to injury is unknown, it is clear that not all cell types are affected similarly by injury and this differential vulnerability leads to circuit dysfunction and behavioral impairment. Importantly, reinstatement of the E/I balance in the hippocampus has been shown to ameliorate mTBI-induced cognitive impairments, demonstrating that these circuit level alterations are critical to memory behavior and may provide an important therapeutic target to ameliorate post-injury memory deficits (Cole et al., 2010).

One of the primary deficits observed in mTBI survivors is memory impairment, including deficits in working memory (McAllister et al., 2001; 2006). Working memory is the ability to hold and manipulate information in mind in order to execute a specific goal. This is a relatively complex cognitive task, requiring the integration of past information, present conditions and desired future outcomes. Working memory is ubiquitous and imperative to carry out everyday activities as well as activities requiring higher level cognitive demands. Additionally, working memory has been shown to contribute to the development of more long-lasting episodic memories (Ranganath et al., 2005). TBI patients are not only less accurate in tests of working memory, but are slower in performing tasks requiring an increased working memory load (Cazalis et al., 2011; Slovarp et al., 2012).

Brain injury induced deficits in memory have been extensively recapitulated using various rodent models of TBI (Lyeth et al., 1990; Creed et al., 2011; Moro et al., 2011). In particular relevance to the work presented here, some of the first research employing LFPI demonstrated post-injury changes in spatial memory performance using the Morris Water Maze (Smith et al., 1991). Following this result, many studies have elaborated on the deficits in spatial memory following LFPI using a variety of behavioral paradigms and time points after injury (Hicks et al., 1993; Dash et al., 2004; Fedor et al., 2010). Similarly, research has shown LFPI animals are outperformed by uninjured animals in working memory tasks like those presented here (Whiting and Hamm, 2006; Hoskison et al., 2009; Eakin and Miller, 2012). Interestingly, imaging evidence has suggested a

disruption in the circuit connecting the hippocampus and the frontal lobe in moderating brain-injury induced deficits in working memory (Wilde et al., 2011).

Interaction between the hippocampus and the prefrontal cortex is critical for spatial working memory function in both humans and rodents (Jones and Wilson, 2005a; Axmacher et al., 2008; Sigurdsson et al., 2010). The anatomical connection between these two spatially distant brain regions was elegantly shown by a series of anatomical experiments in the rat that showed that the hippocampus makes excitatory, glutamatergic, monosynaptic connections with the medial prefrontal cortex (mPFC) (Jay and Witter, 1991; Jay et al., 1992). The connections are primarily ipsilateral, connecting the two structures on the same side of the brain without crossing the midline (Thierry et al., 2000). Though performing many of these anatomical tracing experiments in humans is not feasible, advances in imaging technologies have demonstrated robust functional connectivity between the human orthologs during a working memory task (Petersson et al., 2006).

In rodents, non-match to sample behavior using the T-maze has been established as a task to evaluate spatial working memory behavior that critically depends on the contributions of the prelimbic cortex, a subfield of rodent medial prefrontal cortex. (Thomas and Spafford, 1984; Brito and Brito, 1990; Schwabe et al., 2004). This task requires subjects to choose a stimuli opposite of a recently presented stimuli, after a short delay. Additionally, differences in neuronal firing patterns have been recorded in the mPFC in both primates and rodents when performing non-match to sample working memory tasks (Goldman-Rakic, 1995; Fujisawa and Buzsáki, 2011). However it is clear

that the medial prefrontal cortex is not the only brain structure involved in these spatial working memory tests, and lesioning approaches revealed that both hippocampus and prefrontal cortex are required for working memory (Aggleton et al., 1986; Izaki et al., 2001; Lee and Kesner, 2003; Yoon et al., 2008). Lesioning either structure bilaterally impairs spatial working memory, while disrupting both structures on one side of the brain has no effect of memory performance, presumably because the remaining unaltered pair is sufficient. However, lesioning of the hippocampus on one side and the mPFC on the opposite side of the brain impairs working memory performance, demonstrating that the unilateral connection and interplay between the two regions is necessary for optimal spatial working memory behavior (Floresco et al., 1997; Wang and Cai, 2006).

The physiology of the connection between the hippocampus and mPFC was described soon after its anatomical identification. Stimulation of the hippocampus reliably evokes an action potential in the medial prefrontal cortex of anaesthetized rats, and subthreshold stimulation reveals a fast excitatory postsynaptic potential followed by a slower inhibitory postsynaptic potential (Thierry et al., 2000). Additionally, it was demonstrated that these monosynaptic connections from the hippocampus to the mPFC were able to bi-directionally control synaptic plasticity, further underscoring their potential as a substrate of learning and memory mechanisms (Parent et al., 2010). Moreover, studies in rats performing a spatial navigation task revealed that the phase of theta oscillations in hippocampus modulates the firing probability of mPFC neurons (Siapas et al., 2005). The synchrony between the two regions has been shown to be particularly relevant to their role in working memory function. Synchrony between the regions, as assessed by both coherence (which measures the relation between two signals at the

same frequency in different regions) and phase-amplitude coupling (which measures the relation between the phase of a low frequency oscillation and the amplitude of a high frequency oscillation), increases during the choice phase of the non-match to sample task, peaking as the animal makes a decision (Jones and Wilson, 2005a; Benchenane et al., 2010; Gordon, 2011). Additionally, coherence between the two regions is greater during correct trials and reduced in multiple mouse models of neurological diseases that are accompanied by a deficit in working memory (Jones and Wilson, 2005b; Korotkova et al., 2010; Sigurdsson et al., 2010; Yamamoto et al., 2014).

Though the experimental methods are different, the functional relevance of the hippocampal-prefrontal cortex connection during working memory behavior has also been well documented in humans. Extensive experimentation using functional magnetic resonance imaging has identified increases in the prefrontal cortex (Curtis and D'Esposito, 2003; Courtney, 2004) and the hippocampus (Ranganath and D'Esposito, 2001; Park et al., 2003; Schon et al., 2004) during the delay period of working memory tasks. In these experiments the delay phase is analogous to the choice phase in animal delayed non-match to sample paradigms as the subject is required to maintain a representation of the information in mind during this phase, before executing a goal-directed response at the end of the phase. Additionally, human studies have also detailed the critical role of the interaction between these two regions in supporting working memory, with functional connectivity between the two regions increasing as more objects are required to be held in mind in a task of working memory (Petersson et al., 2006; Rissman et al., 2008). Of relevance to the investigations presented here, children who have suffered a TBI showed a correlation between the severity of

impairment of working memory, and the disruption of this hippocampal-prefrontal functional connection (Wilde et al., 2011).

Unlike the considerable experimental evidence on mTBI induced hippocampal pathology and circuit level alterations, there is a lack of information about putative physiological changes in the prefrontal cortex after mTBI. This is especially surprising since the prefrontal cortex has been shown to be preferentially vulnerable to brain injury by neuropathology studies (Adams et al., 1980), as well as imaging reports (Tong et al., 2004). While studies of TBI survivors have demonstrated alterations including decreased prefrontal activity (Witt et al., 2010) as well as diminished functional connectivity between hippocampus and frontal areas (Marquez de la Plata et al., 2011), the limited previous research carried out using rodent models of mTBI have been limited to morphological (Hoskison et al., 2009) or metabolic changes (Moro et al., 2011) in the mPFC. Therefore in contrast to the hippocampus, there is paucity of experimental evidence from rodent models of mTBI on the level of synaptic circuits, leaving possible physiological substrates of TBI-induced memory impairments unclear. However, some evidence does suggest a possible deficit in inhibitory synaptic transmission in the mPFC (Kobori, 2006).

To address the lack of circuit level of a systematic understanding of post-mTBI alterations to the hippocampus–mPFC circuit, I performed a series of experiments designed to probe how this complicated circuit is altered and potentially impairs memory after LFPI in mice.

First, I investigated working memory using a non-match to sample paradigm in the T-maze in brain-injured as well as sham-operated control animals. This investigation was the first to measure working memory performance in brain-injured animals using a non-match to sample task during the first week after brain injury. These experiments demonstrate persistent working memory impairment throughout the first week after mTBI.

Next, I performed a series of experiments designed to probe circuit level alterations in the mPFC that may be contributing to the observed memory impairment after injury. I investigated mPFC circuit function using a combination of extracellular and intracellular recording in brain slices derived from both brain-injured and sham-operated animals. The data from these experiments demonstrate opposing shifts in synaptic and intrinsic excitability in layer 2/3 of mPFC following mTBI. Interestingly, while the synaptic input to layer 2/3 was significantly altered by mTBI, inputs to layer 5 were unaffected by injury.

To bridge the gap between circuit level investigations performed in brain slices and memory behavior, it is necessary to understand how these circuits function during a memory behavior. To begin to understand the behavioral relevance of the circuit level alterations in both the hippocampus and mPFC I began to develop a framework for recording from these brain structures while animals were performing a memory task. After developing the techniques necessary to produce high-quality recordings of the local field potential, I began my pilot investigations by recording from area CA1 during a

novel object recognition task to provide the basis for future experiments probing spatial working memory after LFPI.

These pilot experiments provide a structure for future *in vivo* recording experiments in awake-behaving animals after LFPI as the methods developed should translate to LFPI animals. Additionally, the pilot experiments generated preliminary data that is similar in structure to anticipated future experiments, which has allowed for the development of a software structure for the complex data analysis that is intrinsic to this type of recording.

Traumatic brain injury is a major cause of cognitive disability. Because mild traumatic brain injury causes memory deficits as its hallmark impairment, these investigations focus on the hippocampus and the medial prefrontal cortex, brain structures critically involved in memory behavior. The work presented here thus adds to our understanding of the circuit level effects of mild traumatic brain injury and provides a framework for future studies to expand our understanding of the aberrant neural activity that underlies memory impairment following mTBI.

# BRAIN INJURY IMPAIRS WORKING MEMORY AND PREFRONTAL CIRCUIT FUNCTION

Colin J. Smith[1,2], Guoxiang Xiong[1], Jaclynn A. Elkind[1], Brendan Putnam[1], Akiva S. Cohen[1]

[1]Research Institute of Children's Hospital of Philadelphia, Philadelphia, PA 19104, USA

[2]Neuroscience Graduate Group, University of Pennsylvania School of Medicine, Philadelphia, PA 19104, USA

## Abstract

More than 2.5 million Americans suffer a traumatic brain injury (TBI) each year. Even mild to moderate traumatic brain injury (mTBI) causes long-lasting neurological effects. Despite its prevalence, no therapy currently exists to treat the underlying cause of cognitive impairment suffered by mTBI patients. Following lateral fluid percussion injury (LFPI), the most widely used experimental model of TBI, we investigated alterations in working memory and excitatory/inhibitory synaptic balance in the prefrontal cortex. LFPI impaired working memory as assessed with a T-maze behavioral task. Field excitatory postsynaptic potentials recorded in the prefrontal cortex were reduced in slices derived from brain-injured mice. Spontaneous and miniature excitatory postsynaptic currents onto layer 2/3 neurons were more frequent in slices derived from LFPI mice while inhibitory currents onto layer 2/3 neurons were smaller after LFPI. Additionally, an increase in action potential threshold and concomitant decrease in firing rate was observed in layer 2/3 neurons in slices from injured animals. Conversely, no differences

in excitatory or inhibitory synaptic transmission onto layer 5 neurons were observed; however, layer 5 neurons demonstrated a decrease in input resistance and action potential duration after LFPI. These results demonstrate synaptic and intrinsic alterations in prefrontal circuitry that may underlie working memory impairment caused by TBI.

## Introduction

Traumatic brain injury (TBI) causes 2.5 million emergency department visits, hospitalizations, and deaths in the U.S. each year and affects millions more that do not seek medical care (Centers for Disease Control and Prevention, 2015). Even mild to moderate traumatic brain injury (mTBI), or concussion, can cause long-lasting cognitive effects including memory impairment (Rutland-Brown et al., 2006). TBI primarily causes damage to the frontal and temporal lobes of the cerebral cortex resulting in persistent cognitive impairment (Stuss, 2011). Functional imaging approaches have described changes to frontal lobe function following TBI (Doshi et al., 2015; Plenger et al., 2015). A common complaint among mTBI sufferers is a loss of working memory, a fundamental ability for maintaining quality of life after mTBI (Stuss et al., 1985; McAllister et al., 2001; Stuss, 2003; Palacios et al., 2012). Despite the prevalence of TBI, post-injury care is palliative and no therapy exists to treat the underlying causes of the cognitive impairments suffered by TBI patients.

Lateral fluid percussion injury (LFPI) is a well characterized and routinely employed rodent model of brain injury that reproduces key features of human TBI including

neuronal cell loss, gliosis, ionic perturbation and memory deficits (Dixon et al., 1987; McIntosh et al., 1987; 1989; Smith et al., 1991). Considerable work in rodent models of TBI has focused on post-injury changes in spatial and working memory performance (Smith et al., 1991; Whiting and Hamm, 2006; Hoskison et al., 2009; Eakin and Miller, 2012). A single mild to moderate LFPI has been shown to induce long-lasting memory impairments, despite a relative lack of neuronal loss, suggesting a circuit mechanism for the observed cognitive deficits (Lyeth et al., 1990). Furthermore, TBI-induced memory impairment has been linked to regionally specific shifts in network excitability in the hippocampus (Witgen et al., 2005), and the hippocampus has been a target of therapeutic interventions designed to reinstate the balance between excitatory and inhibitory synaptic transmission (E/I balance) and restore cognition (Cole et al., 2010).

In contrast to the considerable experimental evidence on mTBI-induced hippocampal pathology, there is a dearth of information regarding putative physiological changes in the prefrontal cortex after mTBI. While human studies of TBI patients have shown changes including decreased prefrontal activity (Witt et al., 2010) as well as diminished functional connectivity between hippocampus and frontal areas (Marquez de la Plata et al., 2011), previous research in rodent models of TBI focused on the prefrontal cortex have centered on morphological (Hoskison et al., 2009) or metabolic changes (Moro et al., 2011). Moreover, investigations into working memory after TBI have examined long-term impairments (>7days) and therefore have trained and tested experimental subjects weeks after injury (Whiting and Hamm, 2006; Hoskison et al., 2009; Eakin and Miller, 2012). The current study is, to our knowledge, the first report to assess working memory impairment using a non-match to sample behavioral paradigm in the days immediately following mild to moderate LFPI.

Interaction between the hippocampus and the prefrontal cortex is critical for spatial working memory function in both humans and rodents (Jones and Wilson, 2005a; Axmacher et al., 2008; Sigurdsson et al., 2010). Specifically, non-match to sample behavior in rodents using the T-maze has been established as a task to evaluate working memory behavior that critically depends on contributions of the prelimbic cortex (Thomas and Spafford, 1984; Brito and Brito, 1990; Schwabe et al., 2004). Additionally, differences in neuronal firing patterns have been recorded in the mPFC in both primates and rodents when performing non-match to sample working memory tasks (Goldman-Rakic, 1995; Fujisawa and Buzsáki, 2011). Altering E/I balance or specifically manipulating miniature excitatory synaptic activity (and thus E/I balance) in prefrontal cortex causes observable changes in behavior (Wang et al., 2011; Yizhar et al., 2011). Layer 2/3 and layer 5 both have critical roles in the functionality of the prefrontal circuit as specific physiological changes in either layer cause changes in behavior (Wang et al., 2011; Hearing et al., 2013; Lee et al., 2015). Furthermore, it is possible the cells in layer 2/3 and layer 5 may have differential responses to injury as is the case with layer specific and cell-type specific changes previously documented in the hippocampus after LFPI (Ross and Soltesz, 2000; Santhakumar et al., 2000; Witgen et al., 2005; Johnson et al., 2014).

In the current study we investigated the physiological correlates of working memory dysfunction after mild to moderate LFPI. We tested for working memory deficits using a non-match to sample behavioral paradigm that critically depends on prefrontal cortex (Kellendonk et al., 2006). Furthermore, using a physiological approach we interrogated the underlying circuitry. That is, we investigated changes in E/I balance, synaptic

transmission, and intrinsic excitability in both layer 2/3 and layer 5 of prefrontal cortex. Our results include a layer-specific series of alterations in both synaptic transmission and intrinsic excitability that may contribute to the working memory dysfunction observed over the first 7 days post-LFPI.

## Methods

### Ethical Approval

All experiments were carried out under protocols approved by the Institutional Animal Care and Use Committee of Children's Hospital of Philadelphia and the guidelines established by the NIH *Guide for the Care and Use of Laboratory Animals*. Experiments were performed on 8 to 12 week old male C57/BL6 mice (Jackson Laboratory, Bar Harbor, ME. Stock number 000664). Experiments were designed to minimize the number of animals required and those used were cared for, handled, and medicated as appropriate to minimize their suffering. Separate cohorts of animals were used for behavioral and *ex vivo* electrophysiological experiments due to the significantly larger number of animals needed for electrophysiological experiments. A total of 120 mice were used in the experiments presented herein.

### Lateral fluid percussion injury (LFPI)

After anaesthetizing the animal with a mix of ketamine (2.6 mg/kg) and xylazine (0.16 mg/kg) via intraperitoneal injection, the animal was placed in a stereotaxic frame (Stoetling, Wood Dale, IL), the scalp was opened, and the fascia scraped from the skull.

An ultra-thin Teflon disc, with the outer diameter equal to the inner diameter of a trephine, was glued to the skull midway between Bregma and Lambda, between the sagittal suture and the lateral ridge on the right side of the skull. Using a trephine, a 3 mm diameter craniectomy was performed over the right parietal area. Following craniectomy, a Luer-loc needle hub (3 mm inner diameter) was secured above the skull opening. Finally, the animal was sutured and placed on a heating pad until mobile, at which point it was returned to its home cage. The next day, the animal was placed under isoflurane anesthesia until it reached a surgical plane of anesthesia (one respiration per 2s). At this point the animal was removed from isoflurane, the hub was filled with saline and connected to the fluid percussion injury device via high-pressure tubing. The animal was placed on its left side on a heating pad. Once a normal breathing pattern resumed, but before sensitivity to stimulation, the injury was induced by a brief (20 ms) pulse of saline onto the intact dura. The peak pressure was monitored with an oscilloscope and for all injuries ranged from 1.4 to 2.0 atm. Immediately after injury the hub was removed from the skull and the animal was placed in a supine position. After righting, the animal was placed under isoflurane to suture the scalp, then placed on a heating pad until mobile, at which point it was returned to its home cage. Sham animals received all of the previously described steps except the fluid pulse.

This type of LFPI is designed to produce a mild to moderate brain injury modeling a non-penetrating concussive injury, as the dura mater is not breached during the procedure. Animal righting time is used as an acute assessment of injury severity and animals with an excessive righting time were excluded from further study (Morehead et al., 1994). The severity of LFPI used here results in hippocampal-dependent cognitive impairment as demonstrated by previous studies employing contextual fear conditioning (Witgen et

al., 2005; Lifshitz et al., 2007; Cole et al., 2010) as well as a significant reduction in neurons in all subregions of the ipsilateral hippocampus as measured using unbiased stereology (Witgen et al., 2005).

**T-maze behavioral paradigm**

In order to motivate animals for food reward, animals used in behavioral experiments were placed on a restricted diet and maintained at 90% of their free-feeding body weight for the duration of the experiment. While in the T-maze mice were rewarded with Reese's Peanut Butter Chips (The Hershey Company, Hershey, PA). Mice were placed on the restricted diet for three days before beginning training, at which time they were allowed to acclimate to the T-maze for ten minutes per day during a free exploration period with all parts of the maze available and no reward present. Subsequently, mice were trained on a non-match to sample behavioral task using a standard T-maze (Dimensions: all arms 7 cm wide x 12.5 cm height. Lengths: start box 17 cm, center arm 31 cm, reward arms 37.5 cm. Med Associates, St. Albans, VT). Each trial consisted of a sample phase, a delay phase, and a choice phase (for schematic see Fig. 1A). The animal began each trial in the start box, at the bottom of the "T". During the sample phase either the left or right arm of the T-maze was blocked, and the animal was rewarded for exiting the start box and proceeding to the end of the maze. The animal was returned to the start box for the delay phase, which in this study was a nominal 0 seconds, to provide a fairly easy working memory task as in (Fujisawa and Buzsáki, 2011). The door separating the start box and the middle arm of the T-maze was lifted beginning the choice phase, during which both goal arms were available. The animal was required to choose the opposite arm to which it was exposed in the sample phase in

order to obtain a reward, which it was allowed to eat for ~5 seconds. If it chose incorrectly it was removed from the maze without receiving a reward. The task requires the animal to retain a memory trace of the sample phase until the point at which it selects an arm during the choice phase. An animal was determined to have chosen an arm once the entire body of the animal including tail entered the arm. Training lasted 7 days immediately preceding LFPI or sham operation after which testing took place for 7 days (10 trials/day). The 10 trials/day consisted of five left-sample and five right-sample trials, presented in pseudo-randomized order. Throughout the duration of the testing phase the experimenter was blinded to animal condition (i.e. whether the animal had received an LFPI or sham procedure). Animals that averaged <60% correct trials over the last three days of training were excluded from analysis as they had not met the criterion for learning the non-match to sample rule. Sixteen mice were used for the behavioral data presented here (n=9 sham-operated animals, n=7 LFPI animals).

**Electrophysiology**

All recordings were made 6-8 days after LFPI or sham operation. Mice were anesthetized with isoflurane, and the brains were quickly and carefully removed, then placed into ice-cold oxygenated (95% $O_2$/5% $CO_2$) sucrose ACSF containing (in mM): sucrose 202, KCl 3, $NaH_2PO_4$ 1.25, $NaHCO_3$ 26, glucose 10, $MgCl_2$ 1, $CaCl_2$ 2. Slices 350 µM thick were cut on a VT1200S vibratome (Leica Microsystems Inc., Buffalo Grove, IL) and transferred to 33-37˚C normal ACSF containing (in mM): NaCl 130, KCl 3, $NaH_2PO_4$ 1.25, $NaHCO_3$ 26, glucose 10, $MgCl_2$ 1, $CaCl_2$ 2, for at least one hour.

*Brain slice selection criteria*

All experiments were performed in the prelimbic cortex, a subfield of rodent medial prefrontal cortex, ipsilateral to the site of brain injury or sham operation. All slices used were from Bregma +1.98 to +1.54 as determined by the presence and shape of the forceps minor of the corpus callosum (Paxinos and Franklin, 2004). Under the microscope, cell layers of prelimbic cortex were easily identifiable. Layer 1 is notable for its lack of cells, while in contrast layer 2/3 contains a dense band of cell bodies. Medial of layer 2/3 there is no layer 4 in this cortical region, while layer 5 is typified by a lower density of larger cell bodies.

*Extracellular recording*

For extracellular recording, electrode internal solution was normal ACSF. The stimulating electrode was placed in layer 2/3, and the recording electrode was placed directly lateral in layer 5 of the prelimbic cortex, as visualized under 4X objective of a BX61WI microscope (Olympus America, Center Valley, PA). Photomicrographs of electrode positions were taken and reviewed post hoc to ensure electrode placement remained consistent across the course of the experiment. In the presence of the NMDA receptor antagonist (2*R*)-amino-5-phosphonovaleric acid (APV; 50 μM) and the AMPA/kainate receptor antagonist 6-cyano-7-nitroquinoxaline-2,3-dione (CNQX; 6 μM) only the fiber volley persisted. In the presence of the voltage-gated sodium channel antagonist tetrodotoxin (TTX; 0.4 μM) both the presynaptic fiber volley and the field excitatory postsynaptic potential (fEPSP) were completely abolished. Both fiber volley and fEPSP measurements are negative-going peak amplitude values in relation to a pre-stimulus

baseline level. (n=20 slices from 12 sham-operated animals, and n=14 slices from 9 LFPI animals)

*Whole-cell patch-clamp recording*

In all whole-cell patch-clamp recordings, only one cell was recorded per brain slice. For whole-cell patch-clamp recording of spontaneous and miniature excitatory postsynaptic currents (sEPSCs, mEPSCs) and intrinsic excitability measures electrode internal solution contained (in mM): K Gluconate 145, HEPES 10, BAPTA 0.1, NaCl 2.5, $MgCl_2$ 2, Mg-ATP 2, GTP-Tris 0.5, and was titrated to a final pH of 7.2-7.3 with KOH. Bicuculline methiodide (30 μM) was added before voltage clamp recordings, and TTX (0.4 μM) was added to isolate mEPSCs. Liquid junction potential of 14.5mV (calculated in Clampex) was corrected for in all data reported from these experiments. Neurons were voltage-clamped at -85 mV for all voltage clamp experiments of excitatory currents (Layer 2/3: n=10 slices from 8 sham-operated animals and n=9 slices from 8 LFPI animals. Layer 5: n=22 slices from 13 sham-operated animals and n=23 slices from 13 LFPI animals). In order to reduce heterogeneity of neurons recorded, experiments began with a series of depolarizing current steps. If neurons fired non-accommodating trains of action potentials followed by large after-hyperpolarizations, they were deemed fast-spiking interneurons and excluded from further analysis. For whole-cell patch-clamp recording of inhibitory currents, internal solution contained (in mM): CsCl 130, $MgCl_2$ 2, HEPES 10, BAPTA 0.1, Mg-ATP 2, GTP-Tris 0.5, and was titrated to final pH of 7.2-7.3 with CsOH. APV (50 μM) and CNQX (6 μM) were added before voltage clamp recordings, and TTX (0.4 μM) was added to isolate mIPSCs. Liquid junction potential of 4.1 mV (calculated in Clampex) was corrected for in all data reported from these

experiments. Neurons were voltage-clamped at -74 mV for all voltage clamp experiments of inhibitory currents (Layer 2/3: n=14 slices from 9 sham-operated animals and n=18 slices from 10 LFPI animals. Layer 5: n=14 slices from 9 sham-operated animals and n=18 slices from 13 LFPI animals).

Patch electrodes with resistances of 4-6 MΩ were pulled from borosilicate glass (World Precision Instruments, Sarasota, FL). Series resistance was monitored throughout the experiment and recordings were discontinued if series resistance exceeded 25 MΩ at any point. Series resistance was compensated for at 80% compensation. All recordings were made using a Multiclamp 700B (Molecular Devices, Palo Alto, CA) sampled at 20 kHz, filtered at 2.4 kHz. Electrophysiological data was analyzed using Clampfit 10 (Molecular Devices) and MATLAB R2012b (Mathworks, Natick, MA). Synaptic events were determined via the Template Search algorithm in Clampfit 10.

*Intrinsic Excitability Measures*

Resting membrane potential was computed as the average voltage in the first two seconds immediately after whole-cell configuration was achieved. All other intrinsic excitability measures were computed from current clamp recordings consisting of a series of ten 500 ms current steps, from -50 pA to 175 pA in 25 pA increments. Constant holding current was applied to maintain the neuron at -85 mV before/after current steps. Action potential threshold was computed by taking dV/dt of the voltage record in the intrinsic excitability experiments described in figures 4 and 6. Threshold was defined as the point where dV/dt first exceeded 30 mV/ms (Howard et al., 2007). Input resistance was determined from the steady-state voltage response to the two hyperpolarizing steps

(-50 pA, -25 pA) and the first depolarizing step (25 pA) (Layer 2/3: n=17 slices from 9 sham-operated animals and n=12 slices from 8 LFPI animals. Layer 5: n=20 slices from 12 sham-operated animals and n=14 slices from 9 LFPI animals).

**Immunohistochemistry**

Seven days after LFPI or sham procedure animals used in behavioral experiments were anesthetized with 5% chloral hydrate and perfused with 10 ml of saline, followed by 50 ml of paraformaldehyde (4% in phosphate buffer, pH 7.4; Sigma-Aldrich). Brains were post-fixed for 90 min at room temperature (RT) and 50 µm thick frontal (also known as coronal) sections were cut with a VT1000S vibratome (Leica Microsystems Inc.). For GFAP staining, sections were incubated with a rat monoclonal antibody (ascetic fluid) against GFAP (1:2 in phosphate-buffered saline [PBS]; gift from Dr. Judith Grinspan) before visualization with Alexa Fluor 488–conjugated goat anti-rat IgG (1:200 in PBS; Molecular Probes). Primary antibody incubation was applied for 90 minutes at RT and continued overnight at 4°C, and the secondary antibody for 90 minutes at RT. Immunostained sections were counterstained with Hoechst. Confocal images were acquired with the Olympus Fluoview 1000 System (Olympus America), with the Z-step kept at 0.5 µm. Consistent confocal settings (laser intensity, confocal aperture, photomultiplier tube, gain, offset, and resolution) were optimized and remained unchanged during the imaging of slices from both sham and LFPI animals.

**Statistics**

In analyzing the T-maze behavioral data, we controlled for individual variations in animal performance (i.e. the animal's ability to perform the behavior before injury or sham procedure) by creating a measure we termed "Memory Performance". We defined Memory Performance as the difference between the animal's percent trials correct on the 3 days preceding LFPI or sham procedure and the percent trials correct on the post-injury day in question, thus negative scores of Memory Performance are associated with a decrease in working memory ability. All behavioral data were confirmed to be Gaussian by D'Agostino-Pearson omnibus tests, and evaluated using Student's t-tests.

Comparison of fEPSP data between LFPI mice and sham-operated controls was assessed in two ways. First, error ellipses demarcating the 95% confidence region of the group data at each stimulation intensity were generated with non-overlapping regions demonstrating significant differences. Additionally, we performed a non-parametric permutation based bootstrapping analysis designed to correct for multiple comparisons. The bootstrapping analysis also allowed us to assess the fiber volley amplitude at which the fEPSP response was significantly different between LFPI mice and sham-operated controls. All individual data were initially pooled, and subjects were then randomly assigned to two groups with the same sizes as the initial comparison. Mean fiber volley and fEPSP amplitudes were computed at each stimulation intensity for each group. An exponential line of best fit was subsequently drawn through the mean data for each group. Next, the difference in fEPSP amplitude between the two fits was computed at intervals of .01 mV of fiber volley amplitude. This procedure was repeated 500 times thus creating a distribution of differences at each value of fiber volley amplitude, spaced by .01 mV. Finally, we performed the comparison using the actual data groups, took the group means, fit them with exponentials, computed the difference between the fits at the

same intervals, and compared the differences to the distributions computed at each interval using a Z-test assessed at a $P<.05$ level. This analysis was performed in MATLAB R2012b (Mathworks).

All comparisons between LFPI mice and sham-operated controls from measures from whole-cell patch-clamp recordings were assessed by Mann-Whitney U tests, or repeated measures ANOVA where appropriate. Prism 6 (GraphPad Software, La Jolla, CA) or SPSS 21 (IBM, Armonk, NY) was used to perform these comparisons. In group data plots assessed by Mann-Whitney U tests, the median is presented. In group data plots assessed by repeated measures ANOVA, means and standard errors of the mean are presented.

## Results

### LFPI produces working memory deficits in the T-maze

In order to assess the effect of brain injury on working memory we performed a delayed non-match to sample task in the T-maze. By pre-training mice before injury, we were able to assess the ability to encode and retain a brief spatial memory trace, rather than the ability to learn the "rule" governing the behavioral paradigm. After training mice to perform the task, one subset of the mice received an LFPI, while the remaining mice received a sham procedure. We then tested the mice in this paradigm for the next 7 consecutive days (for details see Methods). In an effort to determine whether brain injury affected working memory following LFPI, we combined the data from day 1-7 post injury, and compared LFPI animals working memory performance to that of sham-operated

controls. This revealed the decreased ability of brain-injured animals in this working memory task in the first week after brain injury (Sham 0.050 +/- 0.017, LFPI -0.048 +/- 0.023, *P*=0.0008, Fig. 1B). Next, we sought to determine whether the effects of injury were sustained and persisted into the second half of the post-injury testing period. In order to assess this, we binned the data into early (days 1-3 post-injury) and late (days 4-7 post-injury) periods after injury. We found that brain-injured mice showed a reduced ability in the working memory task at both early and late periods post injury (Early: Sham 0.030 +/- 0.022, LFPI -0.067 +/- 0.35, *P*=0.018. Late: Sham 0.065 +/- 0.026, LFPI -0.033 +/- 0.030, *P*=0.016, Fig 1C).

**LFPI reduces network excitability in prefrontal cortex**

Proper functioning of neuronal circuits requires a balance between synaptic excitation and inhibition (E/I balance). To assess potential changes in E/I balance on a network level, we performed extracellular recordings in medial prefrontal cortex (mPFC) an area that has been shown to be important for working memory in the T-maze non-match to sample paradigm as well as similar behavioral tasks (Touzani et al., 2007; Sigurdsson et al., 2010; Cui et al., 2011). We stimulated layer 2/3 of the mPFC and measured the extracellular response in mPFC layer 5. The signal that is produced has two components: the fiber volley, reflecting presynaptic action potentials, and the field excitatory postsynaptic potential (fEPSP), which results from voltage changes in the postsynaptic dendrites (Fig. 2A). We stimulated over a range of intensities, thereby producing an input-output curve. We observed a reduction in the fEPSP after LFPI, without a significant change in the size of the fiber volley (Fig. 2B), indicating that the decrease in the fEPSP was not due to a reduction in the number of afferent fibers

stimulated. Data was analyzed both through the generation of 95% confidence interval (CI) error ellipses and a permutation based bootstrapping analysis in order to correct for multiple comparisons (for details see Methods). Both analyses revealed a decrease in fEPSP amplitude in slices derived from LFPI animals, demonstrating a significant decrease in network excitability in the mPFC in response to LFPI.

**LFPI-induced changes in synaptic transmission in layer 2/3 of prefrontal cortex**

To investigate the source of the LFPI-induced decrease in network excitability described above, we performed a series of whole-cell patch-clamp recordings to measure spontaneous and miniature postsynaptic currents. Miniature currents were isolated by addition of tetrodotoxin to the extracellular solution, thereby eliminating action potentials. Increases or decreases in miniature excitatory currents in the mPFC have been shown to play a role in behavior (Wang et al., 2011) and we hypothesized that these action potential independent currents may contribute to the observed changes in working memory and network excitability.

In brain slices derived from LFPI mice the frequency of spontaneous excitatory postsynaptic currents (sEPSCs) onto layer 2/3 neurons was increased (95% CI Sham 0.913-2.93 Hz, LFPI 2.48-5.05 Hz, $P$=0.0133, Fig. 3B). The frequency of miniature excitatory postsynaptic currents (mEPSCs) also increased in slices derived from LFPI animals (95% CI Sham 0.897-2.81 Hz, LFPI 2.36-3.79 Hz, $P$=0.0431, Fig. 3C). There was no change in the amplitudes of sEPSCs (95% CI Sham 7.675-13.72 pA, LFPI 6.698-15.37 pA, $P$=0.7655, Fig. 3D), or mEPSCs (95% CI Sham 7.294-11.42 pA, LFPI 6.758-8.837 pA, $P$=0.1883, Fig. 3E). Similarly the charge transfer of the currents, as

assessed by the area under the curve, was unchanged by injury (sEPSCs; 95% CI Sham 32.70-52.51 pA*ms, LFPI 32.19-55.89 pA*ms, *P*>0.9999. mEPSCs; 95% CI Sham 33.30-44.24 pA*ms, LFPI 29.73-43.76 pA*ms, *P*=0.6706, data not shown). Conversely, the frequency of spontaneous inhibitory postsynaptic currents (sIPSCs, 95% CI Sham 2.98-4.94 Hz, LFPI 3.03-4.86 Hz, *P*=0.7724) and miniature inhibitory postsynaptic currents (mIPSCs, 95% CI Sham 2.96-3.94 Hz, LFPI 3.05-4.48 Hz, *P*=0.5528) were unaffected by LFPI (Fig. 3F, H, I). However, the amplitude of sIPSCs (95% CI Sham 18.68-22.62 pA, LFPI 16.35-19.85 pA, *P*=0.0489) and mIPSCs (95% CI Sham 17.61-21.51 pA, LFPI 14.96-18.96 pA, *P*=0.0350) were decreased in slices derived from LFPI mice (Fig. 3G, J, K). The charge transfer of sIPSCs was decreased in LFPI mice (95% CI Sham 182.9-234.0 pA*ms, LFPI 132.9-178.1 pA*ms, *P*=0.0078, data not shown). However, the charge transfer of mIPSCs was not significantly different in LFPI mice (95% CI Sham 174.2-215.4 pA*ms, LFPI 150.9-196.2 pA*ms, *P*=0.1306, data not shown).

**Intrinsic excitability of layer 2/3 neurons is affected by LFPI**

Neuronal excitability is influenced by both afferent synaptic excitation/inhibition balance as well as the intrinsic excitability of the neuron itself, which is chiefly determined by the neuron's own cohort of membrane proteins and their activity. In order to assess the intrinsic excitability of layer 2/3 neurons, we subjected each neuron to a series of hyperpolarizing and depolarizing current steps (10 steps, 25 pA, -50 pA to +175 pA, 500 ms, Fig. 4A). Resting membrane potential was unchanged in neurons recorded from LFPI slices (95% CI Sham -68.7--63.4 mV, LFPI -70.1--59.9 mV, *P*=0.9093, Fig. 4B). Input resistance was similarly unaffected by LFPI (95% CI Sham 226.2-294.3 MΩ, LFPI

161.9-285.4 MΩ, *P*=0.2328, Fig. 4C). However, neurons in slices derived from LFPI animals responded with significantly fewer action potentials in response to varying levels of current injection (*F*(1,28)=4.469, *P*=0.044, Fig. 4D) and the action potential threshold was elevated in slices derived from LFPI animals (95% CI Sham -53.2--48.9 mV, LFPI -48.4--43.6 mV, *P*=0.0022, Fig. 4E). However, action potential duration, as determined by the half-width, was unaffected by LFPI (95% CI Sham 1.645-2.002 ms, LFPI 1.713-2.131 ms, *P*=0.3674, Fig. 4F) as was action potential height (95% CI Sham 106.7-117.1 mV, LFPI 104.2-120.2 mV, *P*=0.9761, data not shown).

**LFPI does not affect spontaneous synaptic transmission in layer 5 of prefrontal cortex**

In order to test whether the output of layer 2/3 neurons was maintained after LFPI we recorded spontaneous and miniature excitatory currents in layer 5 neurons. The intra-cortical projection from layer 2/3 to layer 5 is well established, by its ability to generate fEPSPs resembling those evoked in Schaffer collaterals and recorded in stratum radiatum of CA1 (Huang et al., 2004), classical labeling studies using retrograde tracers (Kritzer and Goldman-Rakic, 1995) and paired recording (Morishima and Kawaguchi, 2006; Dembrow et al., 2010). We hypothesized that there would not be any change in sEPSCs in layer 5 after LFPI, despite the increase in excitatory activity onto layer 2/3 neurons due to the elevation of the action potential threshold in the layer 2/3 neurons following LFPI.

In contrast to layer 2/3, and in support of the prediction, all measured parameters of sEPSCs remained unchanged in brain slices derived from LFPI mice (Frequency; 95%

CI Sham 2.45-4.65 Hz, LFPI 2.86-4.87 Hz, *P*=0.6154. Amplitude; 95% CI Sham 7.385-10.26 pA, LFPI 8.074-11.69 pA, *P*=0.4855. Area; 95% CI Sham 35.73-60.36 pA*ms, LFPI 40.58-52.95 pA*ms, *P*=0.6712, Fig. 5B, D). Similarly, parameters of mEPSCs were unaffected by LFPI (Frequency; 95% CI Sham 1.82-3.86 Hz, LFPI 1.76-3.74 Hz, *P*=0.7036. Amplitude; 95% CI Sham 6.790-8.567 pA, LFPI 7.202-9.666 pA, *P*=0.4614. Area; 95% CI Sham 37.16-44.07 pA*ms, LFPI 36.60-46.73 pA*ms, *P*=0.7581, Fig. 5C, E). We also measured inhibitory currents in layer 5 neurons, as we hypothesized there may be a change in feed-forward inhibition onto layer 5 neurons. However, all measured parameters of sIPSCs (Frequency; 95% CI Sham 4.43-5.83 Hz, LFPI 4.15-5.59 Hz, *P*=0.6564. Amplitude; 95% CI Sham 20.20-24.53 pA, LFPI 21.36-33.47 pA, *P*=0.1311. Area; 95% CI Sham 207.7-266.0 pA*ms, LFPI 220.0-351.1 pA*ms, *P*=0.2083, Fig. 5G, I) and mIPSCs (Frequency; 95% CI Sham 3.36-4.43 Hz, LFPI 3.26-4.58 Hz, *P*=0.9183. Amplitude; 95% CI Sham 18.56-23.07 pA, LFPI 18.98-22.50 pA, *P*=0.8029. Area; 95% CI Sham 182.3-228.8 pA*ms, LFPI 192.8-230.1 pA*ms, *P*=0.8685, Fig. 5H, J) remained unchanged as well.

**Intrinsic properties of layer 5 neurons following LFPI**

While the synaptic currents onto layer 5 neurons were not changed following LFPI, membrane proteins in layer 5 neurons may change after LFPI, thus altering cellular intrinsic excitability. In order to examine this possibility we measured intrinsic excitability by injecting the same series of current steps as in the layer 2/3 experiments described in Figure 4 (ten steps, 25 pA, -50 pA to +175 pA, 500 ms).

First, we measured resting membrane potential and found that it was unaffected by LFPI (95% CI Sham -70.5--66.3 mV, LFPI -73.5--67.8 mV, *P*=0.1669, Fig. 6B). We did, however, note a decrease in input resistance of layer 5 neurons after LFPI (95% CI Sham 156.3-220.8 MΩ, LFPI 119.6-162.2 MΩ, *P*=0.0369, Fig. 6C). Generically, a decrease in input resistance results from increased membrane permeability, though it is unclear what the molecular mechanism for this increased permeability may be. We also observed a decrease in the duration of the action potential after LFPI, as measured by action potential half-width (95% CI Sham 1.789-2.099 ms, LFPI 1.550-1.916 ms, *P*=0.0468, Fig. 6F). A decrease in input resistance often results in a decrease in intrinsic excitability, however this was not the case in the layer 5 neurons we recorded. Specifically, the change in input resistance was not accompanied by a change in firing rate ($F(1,33)=.454$, *P*=0.505, Fig. 6D) or action potential threshold (95% CI Sham -52.2--45.5 mV, LFPI -54.4--48.2 mV, *P*=0.2798, Fig. 6E). Action potential height was also unaffected by LFPI (95% CI Sham 103.1-115.3 mV, LFPI 103.9-112.3 mV, *P*=0.6213, data not shown).

**Reactive astrocytosis in ipsilateral but not contralateral mPFC after LFPI**

LFPI produces both focal and diffuse effects, with brain regions immediately under the injury site experiencing the most damage, while more distant parts of the brain, including the contralateral hemisphere, are relatively spared (McIntosh et al., 1989; Thompson et al., 2005; Tran et al., 2006). We predicted that the mPFC is far enough removed from the LFPI site to escape immediate damage from the pressure wave which causes the injury and any circuit deficits observed could be attributed to secondary effects, as is the case in the contralateral hippocampus (Tran et al., 2006). In particular, we reasoned that

if the mPFC was indeed too distant to be directly affected by LFPI, it would not show signs of reactive astrocytosis, which has been shown consistently in the ispilateral hippocampus, but not the contralateral hippocampus following mild to moderate experimental brain injury (Cortez et al., 1989; Chen et al., 2014). We labeled slices from LFPI animals and sham-operated controls with an antibody to glial fibrillary acidic protein (GFAP), a commonly used marker of reactive astrocytosis. Consistent with previous reports employing mild to moderate experimental brain injury, we observed intense GFAP labeling in the ipsilateral hippocampus of LFPI animals (Fig. 7B), while contralateral hippocampus displayed modest GFAP labeling (Fig. 7A). Similarly, modest labeling was observed in the ipsilateral hippocampus in sham-operated control animals (Fig. 7C). In order to examine whether the mPFC experiences a similar increase in reactive astrocytosis as a direct effect of the injury, we performed similar labeling experiments in mPFC. In contrast to our hypothesis, we found intense GFAP labeling in the ipsilateral mPFC of LFPI animals (Fig. 7E) and sparse labeling in the mPFC contralateral to the LFPI (Fig. 7D). In slices from sham-operated controls we observed little or no GFAP labeling (Fig. 7F). This pattern of ipsilateral reactive astrocytosis supports the notion that the effects of injury in the ipsilateral mPFC is similar to that of the ipsilateral hippocampus.

## Discussion

In this study, we demonstrate working memory impairments acutely following mild to moderate LFPI and sustained for 7 days post-injury. Initially, we show a reduction in network excitability in the mPFC, a brain region involved in working memory, 7 days post-injury. Additionally, further experiments reveal shifts in both excitatory and inhibitory

synaptic transmission that are specific to layer 2/3. Furthermore, we present changes in the intrinsic excitability of cells in both layer 2/3 and layer 5 of the mPFC.

Previous reports employing LFPI to describe working memory impairment in rats have focused on later time points (beginning at ~14d) and have shown a delay-dependent deficit, unlike the current study (Whiting and Hamm, 2006; Eakin and Miller, 2012). The experiments presented here were designed to investigate physiological changes within the clinically relevant “therapeutic time window” but after transient changes that subside by 48hrs post-injury (Grady, 1994). Working memory deficits are a constant finding across multiple models of TBI (Milman et al., 2005; Hoskison et al., 2009; Moro et al., 2011), and here we illustrate an acute and enduring impairment of working memory using a common and well characterized experimental model of TBI and species/strain of rodent.

To probe the underlying substrate contributing to the behavioral impairment, we performed experiments that illustrate a series of physiological alterations in mPFC circuitry 7 days after LFPI. Our initial physiological finding, a decrease in network excitability in the mPFC, as shown by the decrease in fEPSPs, demonstrates a shift in E/I balance in this circuit following LFPI. Shifts in E/I balance have been previously reported following LFPI in the hippocampus, and reinstatement of this balance has been effective in restoring hippocampal dependent cognition (Cole et al., 2010). This report is the first to describe E/I imbalances in the mPFC following LFPI.

To examine potential circuit mechanisms that could be contributing to shifts in network excitability after brain injury, we measured both excitatory and inhibitory currents onto

layer 2/3 neurons as well as the intrinsic membrane properties of layer 2/3 neurons. These experiments demonstrated a net increase in the excitatory drive onto layer 2/3 neurons, potentially making these neurons more likely to fire action potentials. However, examination of intrinsic excitability parameters determined that action potential threshold was increased. This produced the opposite effect as layer 2/3 neurons fired less action potentials in response to current injection. This type of compensatory response has been well described in other paradigms (Turrigiano, 2008; 2011) as well as in other brain regions after LFPI (Howard et al., 2007). Unlike the previous work investigating homeostasis after brain injury, which also described opposing shifts in intrinsic excitability and synaptic inputs after LFPI, this study employs behavioral testing to assess the behavioral relevance of these changes. The behavioral data supports the notion that the potential compensatory mechanisms we observed were insufficient in mitigating cognitive impairment, however more experiments will be needed to more fully test this hypothesis. Additionally, further experiments are necessary to verify that post-LFPI alterations in intrinsic excitability are a compensatory response to changes in synaptic input and not a direct effect of the injury itself.

There are multiple biological mechanisms that may contribute to differential vulnerability of layer 2/3 and layer 5 neurons in the mPFC after brain injury. Chiefly, there are two distinct subtypes of excitatory output neurons within the mPFC, pyramidal tract (PT) and intratelencephalic (IT) neurons, which are defined by their projection targets (Molnár and Cheung, 2006; Shepherd, 2013; Dembrow and Johnston, 2014). IT neurons are found in both layer 2/3 and layer 5, while PT neurons are only found in layer 5. Importantly, these two classes of neurons respond differentially to neuromodulators including dopamine and serotonin (Avesar and Gulledge, 2012; Seong and Carter, 2012). Furthermore, IT

neurons and PT neurons express different cohorts of intrinsic membrane channels, which affects the way the two classes of neurons respond to network input and leads to each type having a unique role within the prefrontal circuit (Dembrow et al., 2010; Kalmbach et al., 2013). Modifying these intrinsic properties, specifically h-current, has been shown to cause both improvements and deficits in memory performance (Wang et al., 2007; Thuault et al., 2013). The current study supports a possible preferential alteration of IT neurons to injury. However, the molecular mechanism(s) underlying this sensitivity and the observed insensitivity of PT neurons is a topic for further exploration.

To our knowledge this is the first study describing working memory deficits acutely and continuously throughout the first week after LFPI. The data demonstrate no evidence of recovery of working memory in the seven days following brain injury. Unlike previous studies that have focused on morphological and neurochemical changes, this study assesses physiological correlates of working memory dysfunction in the prefrontal cortex. These results support the hypothesis that injury-induced disruption of E/I balance is a key factor contributing to behavioral impairments. Additionally, our results support the idea that the prefrontal cortex, along with other regions known to be affected by brain injury, plays a role in post-injury memory deficits. Future studies could extend the current investigation into the cellular and molecular mechanisms of the observed changes as well as further bridging the gap between physiology and behavior by recording from the prefrontal cortex in awake-behaving animals after LFPI.

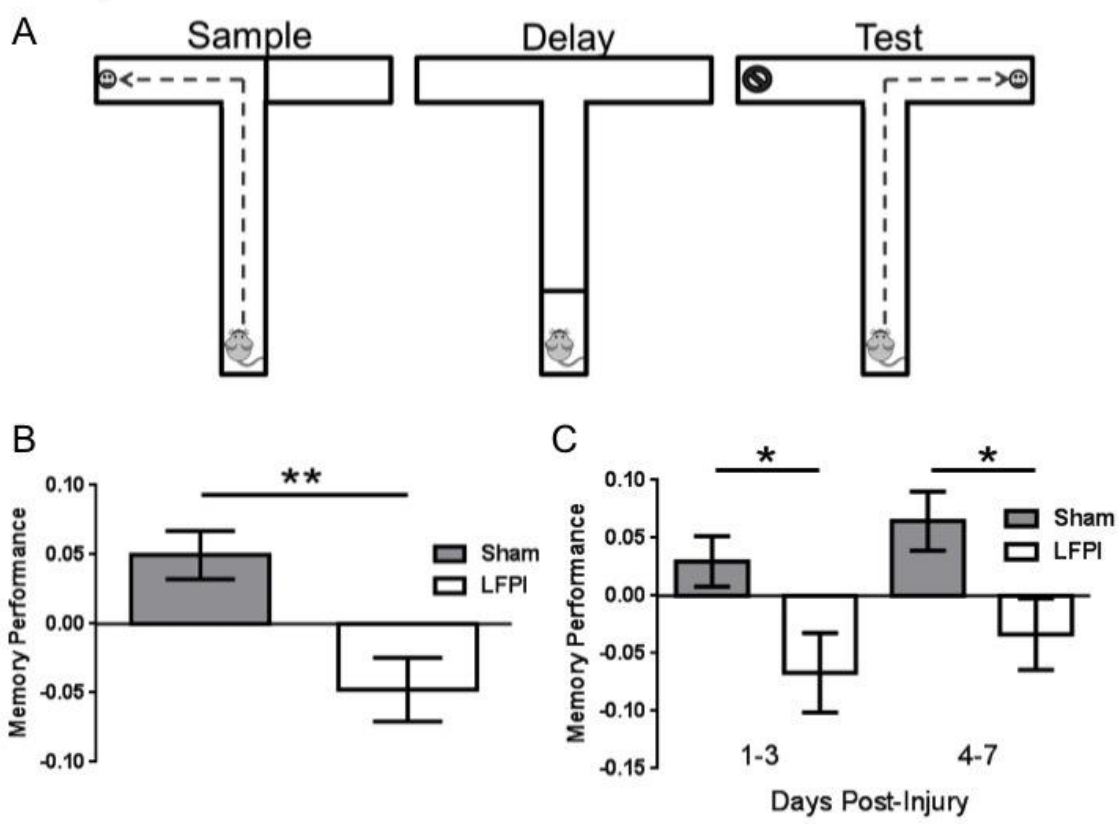


**Figure 1:** ***Persistent working memory impairment immediately following LFPI.*** (A) Schematic of the T-maze and the three phases of a trial. The sample phase exposes the animal to one arm to receive a food reward, then after the delay phase, the animal is exposed to both arms in the choice phase and must select the opposite arm in order to receive a food reward. (B) Memory Performance as assessed by the delayed non-match to sample task, is impaired over the first 7 days after LFPI. (** indicates $P<0.001$) (C) Memory Performance is impaired in both the first three days after LFPI as well as days four through seven after injury (* indicates $P<0.05$).

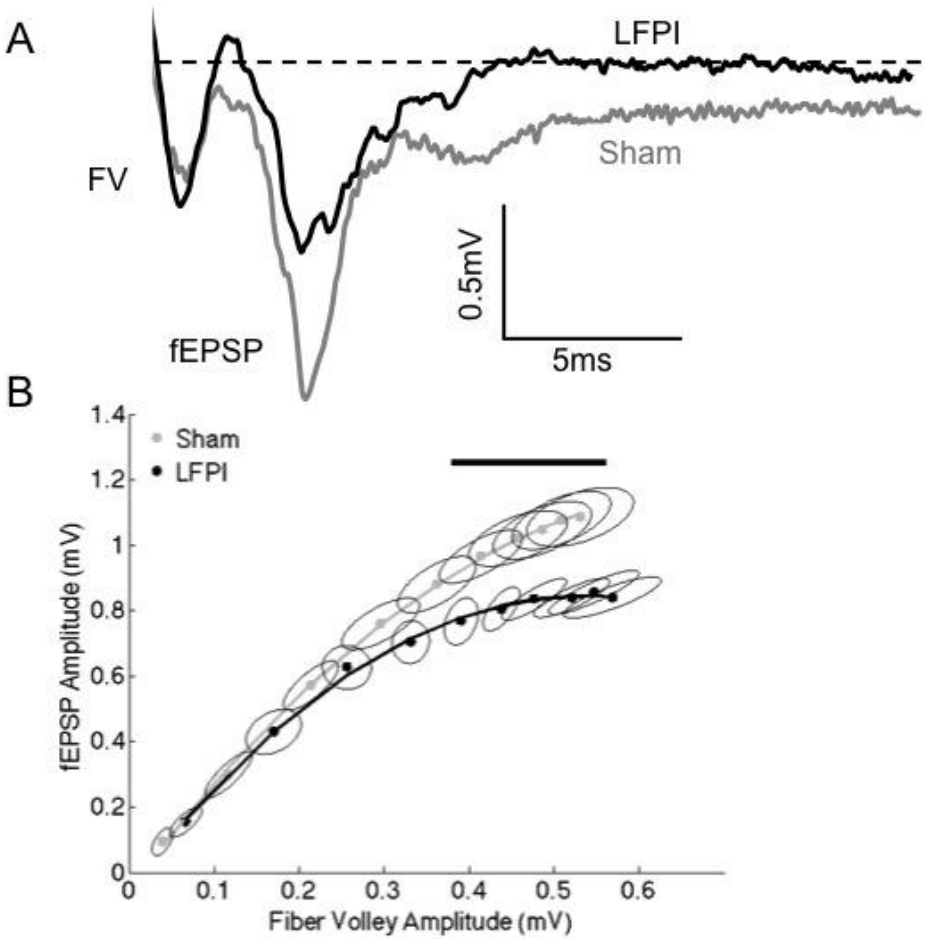


**Figure 2:** ***Decreased field excitatory postsynaptic potentials following LFPI.*** (A) Representative extracellular recordings at the highest stimulation intensity used (300 μA). Fiber volley amplitude is unchanged; however, fEPSP amplitude is reduced in response to LFPI***.*** Dashed line indicates baseline voltage, aligned for both traces. FV denotes fiber volley, fEPSP denotes the field excitatory postsynaptic potential. (B) Fiber volley amplitude and fEPSP amplitude at stimulation intensities ranging from 30-300 μA. Error ellipses indicate the 95% confidence area for each measure. The horizontal line above the data indicates the fiber volley amplitudes for which the groups differ in fEPSP amplitude as assessed by a permutation-based bootstrapping method at the α=.05 level.

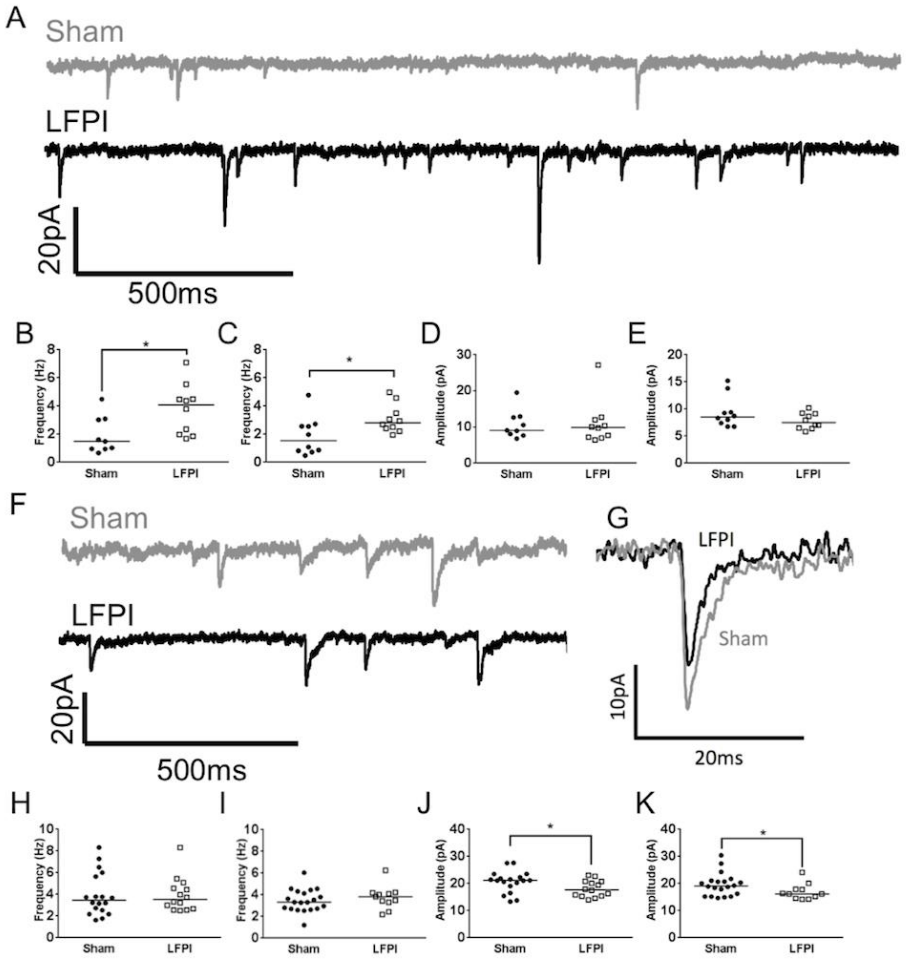


**Figure 3:** ***Shifts in synaptic input onto layer 2/3 following LFPI.*** (A) Representative traces from layer 2/3 mPFC neurons showing sEPSCs, note the increase in frequency of currents in the LFPI trace. (B) Group data illustrating increase in frequency of sEPSCs and (C) mEPSCs in LFPI neurons (* indicates P<0.05). (D) Group data illustrating no difference in amplitude of sEPSCs or (E) mEPSCs following LFPI. (F) Representative traces from layer 2/3 mPFC neurons showing sIPSCs. (G) Representative traces of a single sIPSC of median amplitude. Note the decrease in amplitude after LFPI. (H) Group data illustrating no change in frequency of sIPSCs or (I) mIPSCs in LFPI neurons. (J) Group data illustrating increase in amplitude of sIPSCs and (K) mIPSCs following LFPI (* indicates P<0.05).

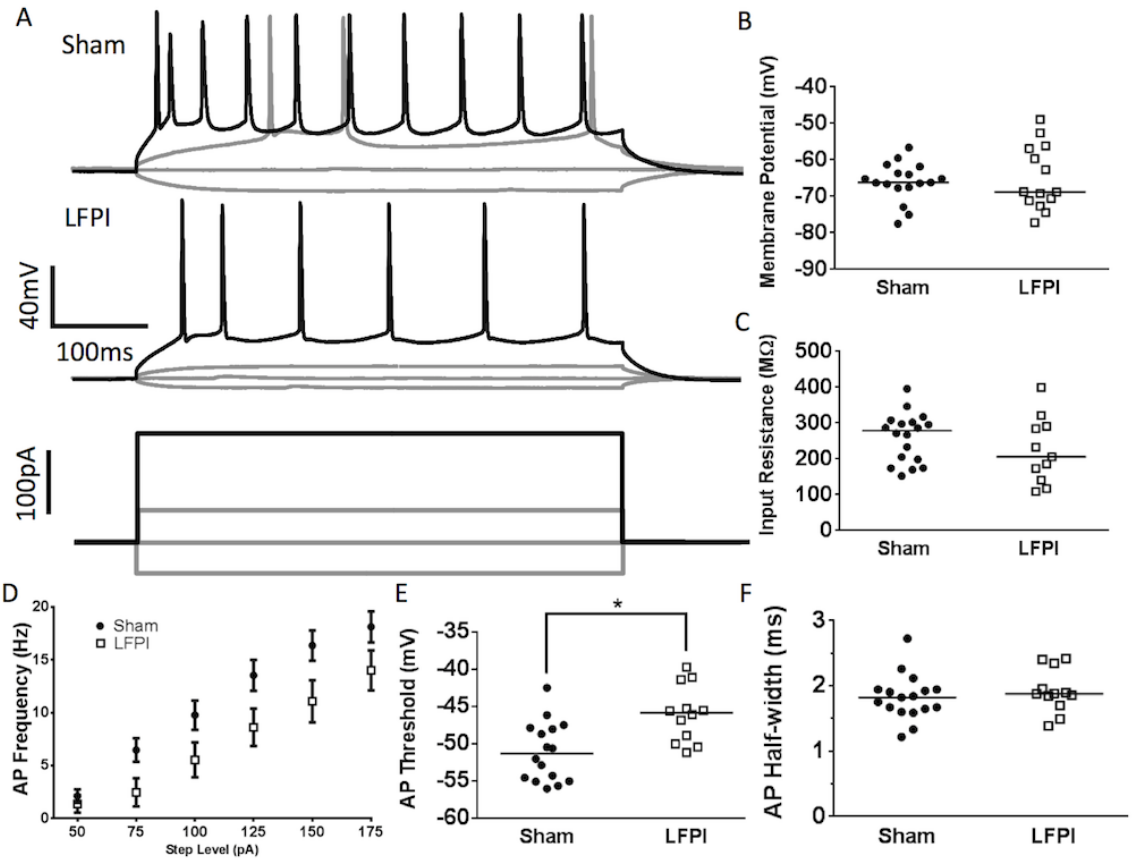


**Figure 4:** ***Alterations in layer 2/3 intrinsic excitability following LFPI.*** (A) Representative traces from layer 2/3 neurons showing voltage response to selected current steps (-50, 0, 50, 175 pA). Response to 175 pA current step shown in black for visual clarity. Note the decreased firing rate in the LFPI trace. (B) Group data displaying no change in resting membrane potential after LFPI. (C) Group data illustrating no difference in input resistance after LFPI. (D) Frequency versus current group data showing an increase in firing rate following LFPI. (E) Action potential threshold is significantly depolarized in slices derived from LFPI animals (* indicates $P<0.05$). (F) Action potential half-width is unchanged following LFPI.

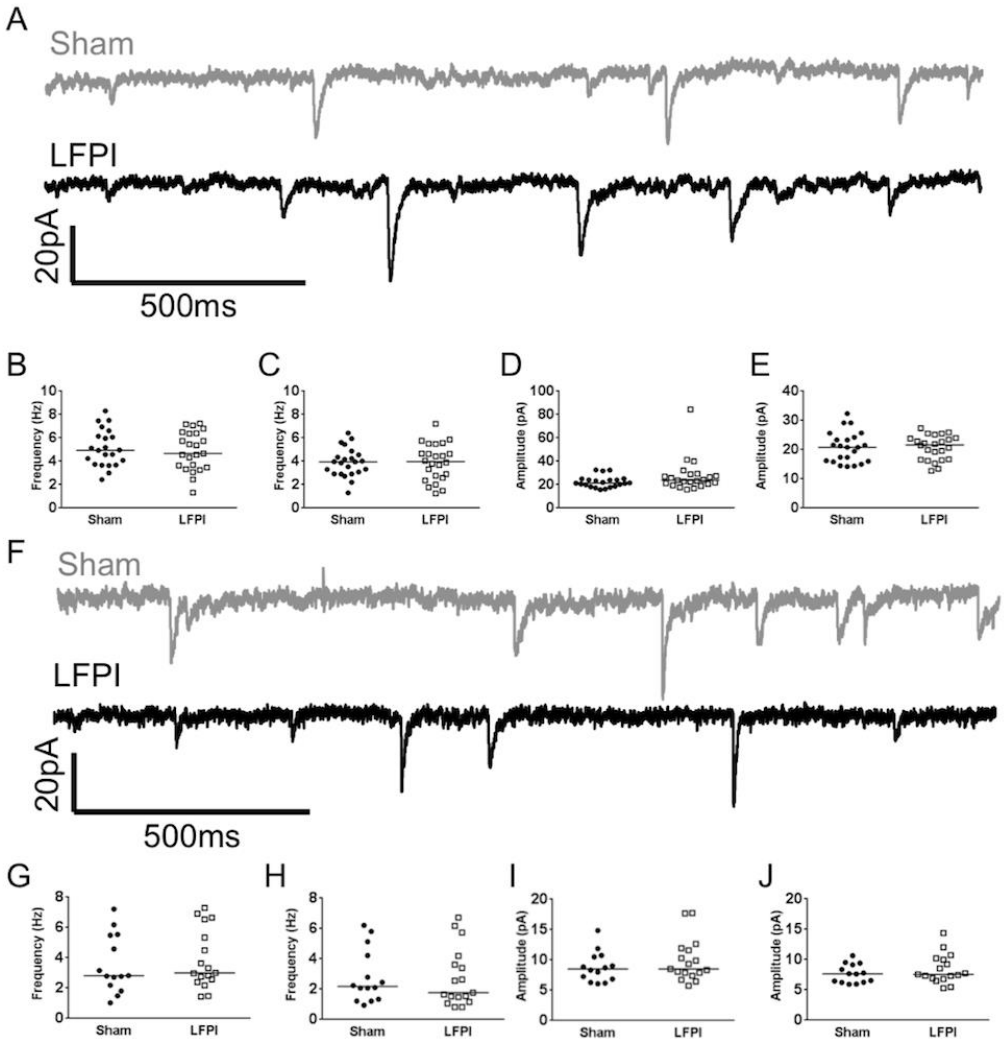


**Figure 5:** ***Synaptic input to layer 5 is unchanged following LFPI.*** (A) Representative traces from layer 5 mPFC neurons showing sEPSCs. (B) Group data illustrating no change in frequency of sEPSCs or (C) mEPSCs in LFPI neurons. (D) Group data illustrating no difference in amplitude of sEPSCs or (E) mEPSCs following LFPI. (F) Representative traces from layer 5 mPFC neurons showing sIPSCs. (G) Group data illustrating no change in frequency of sIPSCs or (H) mIPSCs in LFPI neurons. (I) Group data illustrating no difference in amplitude of sIPSCs or (J) mIPSCs following LFPI.

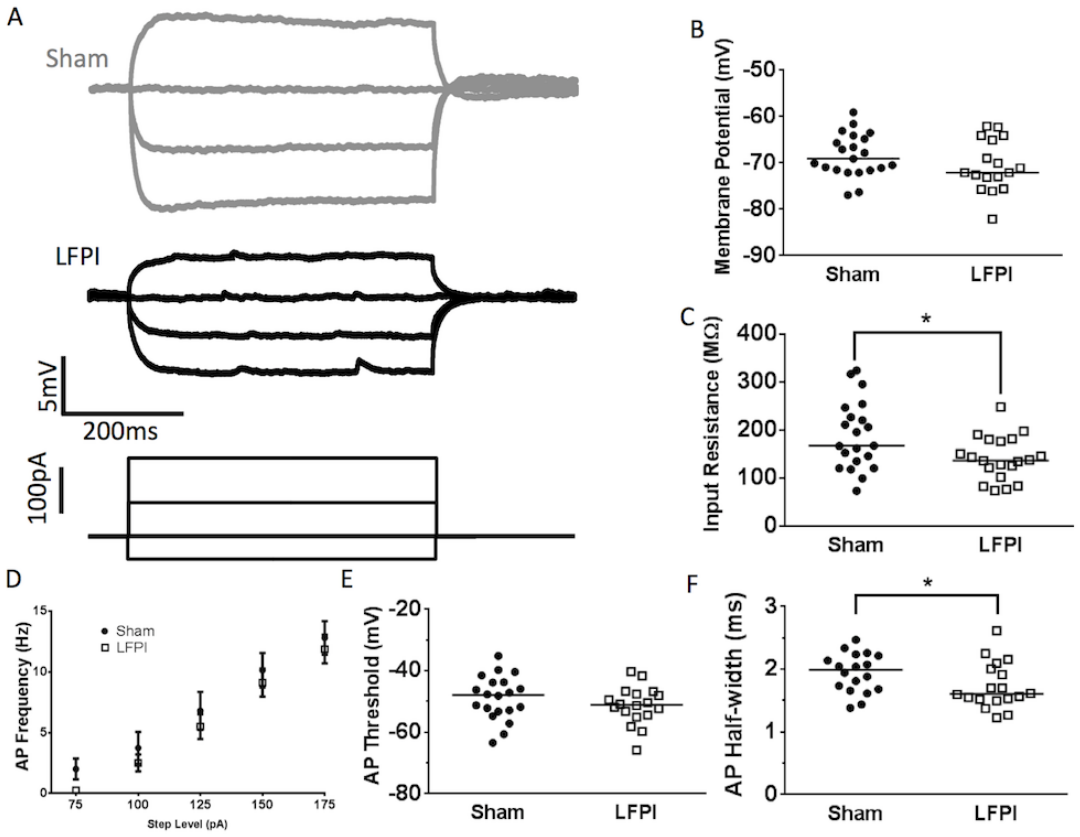


**Figure 6:** ***Input resistance of layer 5 neurons is affected by LFPI.*** (A) Representative traces from layer 5 neurons showing voltage response to selected current steps (-50, -25, 0, 25 pA). (B) Group data displaying no change in resting membrane potential after LFPI. (C) Group data showing a reduction in input resistance in layer 5 neurons after LFPI (* indicates P<0.05). (D) Frequency versus current group data shows no change in firing rate after LFPI. (E) Action potential threshold is unchanged after LFPI. (F) Group data, illustrating significantly shorter action potential half-width following LFPI (* indicates P<0.05).

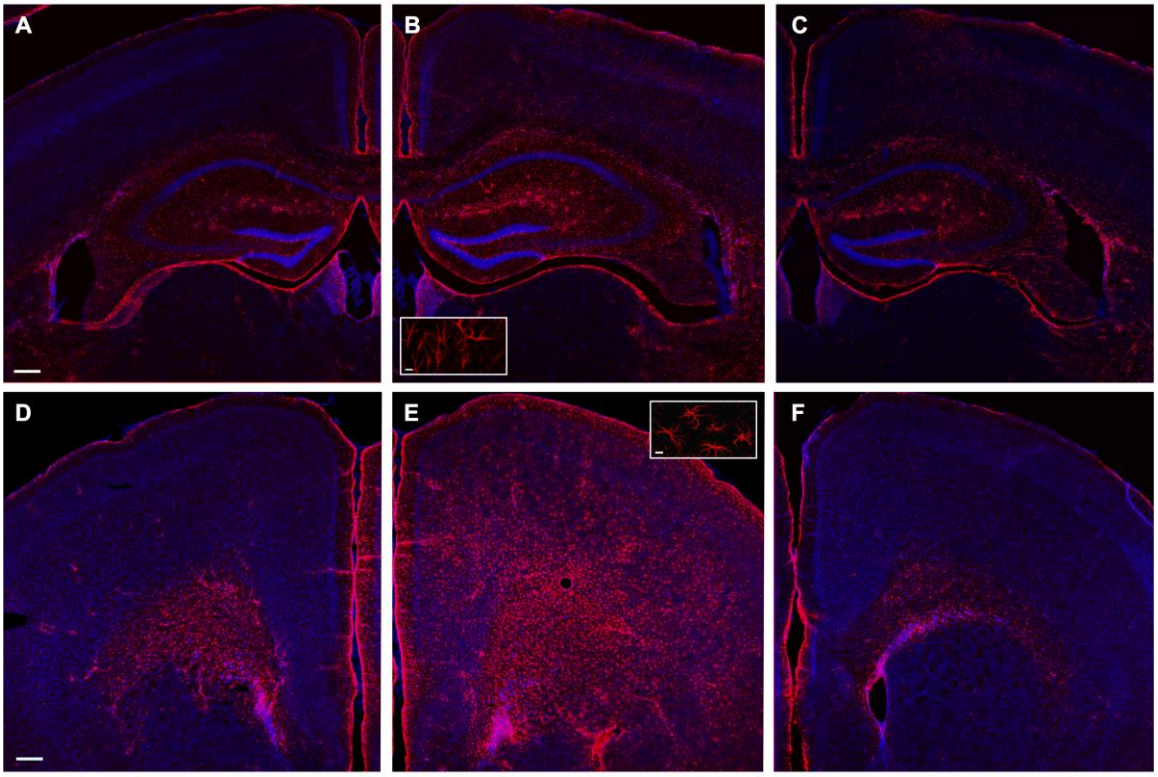


**Figure 7: *GFAP labeling following LFPI*** (A) Example photomicrograph of contralateral hippocampus from LFPI animal (B) Example photomicrograph of hippocampus ipsilateral to LFPI, inset displaying astrocyte morphology. (C) Example photomicrograph of ipsilateral hippocampus from sham-operated animal. (D) Example photomicrograph of contralateral mPFC from LFPI animal (E) Example photomicrograph of mPFC ipsilateral to LFPI, inset displaying astrocyte morphology. (F) Example photomicrograph of ipsilateral mPFC from sham-operated animal. *GFAP labeling in red, Hoescht labeling for DNA in blue. Scale bar in = 200um, inset scale bar = 10um.*

# LOCAL FIELD POTENTIAL RECORDINGS IN AWAKE-BEHAVING ANIMALS: PILOT EXPERIMENTS AND METHOD DEVELOPMENT

Colin J. Smith[a, d], Russell Port[d], Jeffrey Berman[b], Hannah Matheny[a], Akiva S. Cohen[a, c]

[a]Research Institute of Children's Hospital of Philadelphia; Department of Radiology, Children's Hospital of Philadelphia; Department of [c]Anesthesiology and [d]Neuroscience Graduate Group, University of Pennsylvania School of Medicine.

**Abstract**

Understanding the dysfunction of neuronal circuits involved in memory is among the most pressing challenges facing researchers of traumatic brain injury. Here we present pilot experiments and analyses designed to probe dysfunction in neuronal circuits in awake-behaving animals. Sham-operated animals performed a spatial object recognition task designed to engage the hippocampus while we recorded local field potentials from hippocampal area CA1 using chronically implanted tetrode microdrives. These experiments verified the ability of sham-operated mice to successfully complete the task. Furthermore, we demonstrate the ability to record high quality local field potentials from these animals, to separate broadband activity from narrow band neuronal oscillations and to quantify the degree of association between the phase of low frequency oscillations with the amplitude of high frequency oscillations. We anticipate that the

protocols and methods developed here will be critical to future investigations on *in vivo* signatures of brain injury.

## Introduction

Despite considerable interest in memory processes and structures and their role in post-TBI deficits, bridging the gap between *ex vivo* studies of memory circuitry and memory behavior remains difficult. Previous research investigating the various contributions of individual brain regions to memory formation and recall in humans and animal subjects has employed *in vivo* recording of brain activity while subjects perform memory tests, with the goal of correlating specific patterns of brain activity to subject behavior. By recording brain activity in TBI patients as well as rodent subjects who have experienced an experimental TBI, it may be possible to reveal an electrophysiological signature in brain activity that will correlate with both cellular markers of brain injury as well as impaired memory behavior. The development of such an endophenotype of TBI, as has previously been established in schizophrenia (Spencer et al., 2004; Spencer, 2009; Carlson et al., 2011; Hall et al., 2011), would provide a translational biomarker that could be used to assess both human patients as well as rodent laboratory subjects. This would allow more effective therapy development as well as a more reliable tool for diagnosis and return to play guidelines for TBI sufferers.

In order to investigate patterns of brain activity that correlate with post-TBI memory deficits we will investigate brain activity in the hippocampus during spatial object recognition behavior. The hippocampus is an ideal location to probe for post-TBI deficits in *in vivo* physiology as its role in memory behavior is well established (Scoville and

Milner, 1957; Squire and Zola-Morgan, 1991; O'Keefe, 1993; Squire et al., 2004). Also importantly, the hippocampus is known to be selectively vulnerable to damage following traumatic brain injury (Skelton et al., 2000; Tate and Bigler, 2000; Arciniegas et al., 2001; Bigler et al., 2002; Umile et al., 2002) and this specific vulnerability is recreated/mimicked by the experimental model of brain injury employed here i.e., lateral fluid percussion injury (LFPI) (Smith et al., 1991; Santhakumar et al., 2002; Witgen et al., 2005; Bonislawski et al., 2007). Performing *in vivo* recordings in the hippocampus of awake-behaving rodents is well established, and therefore it will be comparatively easy to adapt previously used recording methods to our purposes. We will record oscillations of the local field potential using depth electrodes, in this case four tetrodes implanted via microdrives. Oscillations of the local field potential (LFP), are well established as a neural correlate of excitatory/inhibitory synaptic balance (Atallah and Scanziani, 2009) a neural metric we have investigated in many previous *ex vivo* studies (Witgen et al., 2005; Cole et al., 2010; Johnson et al., 2014). Furthermore, in investigating the hippocampus we can attempt to correlate hippocampal activity to a memory behavior that is known to be dependent on the hippocampus, spatial object recognition (Ennaceur and Aggleton, 1997; Oliveira et al., 2010; Barker and Warburton, 2011). This behavior involves encoding and recall of an object's spatial location within a behavioral arena and is impaired in animals with hippocampal lesions, as well as animal models of disease states known to alter hippocampal function (Mumby, 2001; Gilbert, 2004; Winters et al., 2008; Wimmer et al., 2012).

While the hippocampus is critical for the specific type of memory investigated in the behavioral experiments described herein, we are also interested in types of memory that require effective interactions between the hippocampus and other memory brain

regions, such as the prefrontal cortex. In order to investigate the relationship between spatially distinct brain regions in effective memory encoding and recall, we plan to use analytical methods such as Phase-Amplitude Coupling (PAC), which examines how the phase of low frequency neuronal oscillations correlate with the amplitude of high frequency neuronal oscillations and can be quantified using signals from two distinct brain regions in order to probe complex interactions between regions.

While *in vivo* recording in the hippocampus in awake-behaving rodents is a well-established technique for investigating memory processes (Tort et al., 2009; Fujisawa and Buzsáki, 2011; Yamamoto et al., 2014), considerably less work has been done in rodent models of TBI. To this point, previous research has demonstrated a post-TBI decrease in neuronal oscillations in the theta band (6-12 Hz) during a working memory task in studies employing a rat model of TBI (Fedor et al., 2010; Lee et al., 2013). Similarly, investigations recording single cell firing rates in rats after TBI during memory tasks have revealed no decrease in the overall firing rate after injury (Eakin and Miller, 2012) but a reduction in bursting activity (Munyon et al., 2014). Compared to the extensive research on the relationship between *in vivo* electrophysiology and memory processes in healthy animals, as well as other disease states such as schizophrenia and epilepsy, this is a relative paucity of literature involving TBI. No research has been done on awake-behaving mice after experimental TBI, nor have studies examined frequency bands outside the theta range, broadband activity, or physiological interactions between brain regions that play a critical role in memory behavior.

In the set of experiments presented here we aimed to pilot the behavioral

paradigms, recording technologies and analytical techniques that we will use to rigorously investigate the open questions that attempt to bridge the exisiting gap between post-TBI physiology and deficits in memory behavior. Specifically, we determined a set of best practices and parameters that allowed us to assess spatial object recognition behavior in the mice while recording their hippocampal activity. We successfully constructed and implanted custom microdrives that allowed us to record local field potentials from hippocampal area CA1 in awake-behaving mice. Lastly, we established a modular analytical pipeline consisting of a series of custom software scripts written in MATLAB for use in analyzing local field potential data generated by the experiments described here. Furthermore, these scripts were constructed to be flexible and modifiable, to ease use in future, similar experiments.

## Materials and Methods

*Subjects*

All experiments were carried out under protocols approved by the Institutional Animal Care and Use Committee of Children's Hospital of Philadelphia and the guidelines established by the NIH *Guide for the Care and Use of Laboratory Animals*. Experiments were performed on 8 to 12 week old male C57/BL6 mice (Jackson Laboratory, Bar Harbor, ME. Stock number 000664). Experiments were designed to minimize the number of animals required and those used were cared for, handled and medicated as appropriate to minimize their suffering.

*Lateral Fluid Percussion Injury*

After anaesthetizing the animal with a mix of ketamine (2.6 mg/kg) and xylazine (0.16 mg/kg) via intraperitoneal injection, the animal was placed in a stereotaxic frame (Stoetling, Wood Dale, IL). The scalp was opened and the fascia scraped from the skull. An ultra-thin Teflon disc, with the outer diameter equal to the inner diameter of a trephine, was glued to the skull midway between Bregma and Lambda, between the sagittal suture and the lateral ridge on the right side of the skull. Using a trephine, a 3 mm diameter craniectomy was performed over the right parietal area. Following craniectomy, a Luer-loc needle hub (3 mm inner diameter) was secured above the skull opening. Finally, the animal was sutured and placed on a heating pad until mobile, at which point it was returned to its home cage. The next day, the animal was placed under isoflurane anesthesia until it reached a surgical plane of anesthesia (one respiration/2s). At this point the animal was removed from isoflurane, the hub was filled with saline and connected to the fluid percussion injury device via high-pressure tubing. The animal was placed on its left side on a heating pad. At this point normally the animal would receive a fluid pulse onto the intact dura which would create a brain injury, however all animals in the investigations presented in this chapter were sham-operated controls, meaning they received no injury. At this point, the hub was removed from the skull and the animal was placed in a supine position. After righting, the animal was placed under isoflurane to suture the scalp, then placed on a heating pad until mobile, at which point it was returned to its home cage.

*Electrode Implantation Surgery*

Seventy-two hours after LFPI or sham procedure, animals were anaesthetized with a mix of ketamine (2.6 mg/kg) and xylazine (0.16 mg/kg) via intraperitoneal injection and placed in a stereotaxic frame. Previously constructed microdrives (Versadrive-4, Neuralynx, Bozeman, MT) consisting of four independently driveable tetrodes were implanted 2.2 mm posterior to bregma, 2 mm lateral to the midline to a depth of 1.7mm beneath the dural surface. The microdrive was permanently attached to the skull with dental cement, after which the animal was placed on a heating pad until mobile, and then returned to its home cage.

*Behavioral Paradigm & Analysis*

All behavioral sessions were completed in the dark. Starting 48 hours after electrode implantation surgery subjects were habituated to the arena (45 x 45 cm with 30 cm walls) and the rest box (15 x 15 cm with 20 cm walls) for 30 minutes each for 5 days. The walls of the arena were dark brown, except for one wall that was white, serving as a local cue. This local cue and the distal cues provided by objects in the behavioral room remained the same during the course of the experiment. After 5 days of habituation, subjects underwent spatial object recognition testing on day 6. Spatial object recognition testing began with a 10 minute session in the rest box, followed by a 10 minute familiarization session (F), where subjects were exposed to identical novel objects placed in diagonally opposed corners of the arena. Following a 5 minute rest session, subjects were reintroduced to the arena for novel location testing (NL) for 5 minutes. During NL one object remained in the same location as in F, while one of the objects was moved to new quadrant of the arena. Objects were thoroughly cleaned with 70%

ethanol in between sessions in order to remove any odorant cues. After NL subjects were returned to the rest box for a 5 minute rest session. Next, the subjects returned to the arena for a 5 minute novel location & object (NLO) testing session. During NLO, the object that did not change location between F and NL remained in its position while a novel object, which the subjects had not experienced in F or NL, was placed in the remaining quadrant where there was no object in F or NL. Finally, the subject was returned to the rest box for a 10 minute rest session (for diagram see Figure 1A).

Memory behavior was assessed by measuring the relative amount of time the subjects spent within 8 cm of the center of the objects. Animal location was tracked via a pair of LEDs attached to the headstage that was plugged in to the microdrive at all times during recording. The LED based tracking allowed for the automation of objective behavioral scoring as the midpoint between the LEDs marked the center of the animal's head. Custom scripts were written in MATLAB in order to compare the time spent near each object in each condition. Specifically, the amount of time the subject spent near the spatially displaced object (in NL sessions) or the novel object (in NLO sessions) was divided by the total time the subject spent near either object. A Novelty Exploration score of 0 indicates the animal only explored the familiar object, a score of 1 indicates the animal only explored the novel object, while a score of 0.5 indicates the animal explored the two objects equally.

*Electrophysiology*

Neural data was collected continuously throughout the behavioral paradigms. The headstage was connected to a tethered unity gain amplifier equipped with green and red LEDs used for tracking the position of the animal. The tether was connected to a 32 channel amplifier (Neuralynx, Bozeman, MT). The amplifier output was digitized at 32.6 kHz. Position of the animal and electrophysiological data were recorded by Cheetah Data Acquisition software (Neuralynx, Bozeman, MT). Electrical signals were filtered between 0.1 and 9,000 Hz.

*Data Processing*

Data was processed in five-minute sessions that corresponded to the length of the behavioral sessions (F, NL, & NLO). In the case of familiarization sessions the final five minutes was used to provide consistency, though the sessions were 10 minutes long. Immediately after the data was imported into MATLAB for analysis, a Z-score was computed for each sample and samples with Z-score absolute value > 5 were deemed artifacts and omitted from further analysis. In order to extract power and phase spectrum from each 5-minute session we convolved the data with a bank of 101 linearly spaced Morlet wavelet filters from 3 to 100Hz, with linearly increasing wavelet cycles from 3 to 6. For power analyses the instantaneous power across the entire behavioral session was computed and then averaged. In order to separate broadband activity from narrowband activity in specific frequency ranges we performed a broadband subtraction based on the methods of (Manning et al., 2009). Briefly, we

logarithmically transformed both the axes of the power spectra (frequency and power) to linearize the data and subsequently fit each individual animal's power spectrum with a robust fit linear regression. The mean of the regression line is taken as a measure of broadband power, while the residuals represent the narrowband power at each frequency (Manning et al., 2009).

*Phase Amplitude Coupling*

In order to determine the extent of the association of the phase of low frequency signals with the power of high frequency signals we quantified Phase-Amplitude Coupling (PAC) with a variable width filter as described in (Berman et al., 2012). Briefly, this method computes the Canolty modulation index (Canolty et al., 2006) but replaces the fixed bandwidth filter with a variable bandwidth filter that is twice the width of the high frequency signal (Berman et al., 2012). The low frequencies (or carrier frequencies) analyzed ranged from 3-14 Hz and the high frequencies (or modulated frequencies) ranged from 15-100 Hz. By computing the modulation index at each possible pair of frequencies and pseudo-coloring higher modulation values with warmer colors we can construct a comodulogram, a visual tool for assessing PAC (for example see Figures 4-6, A-C).

*Sobel edge detection*

To determine the outlines of regions of interest of the phase-amplitude coupling comodulograms in an unbiased manner, the Sobel method of edge detection was implemented in MATLAB. Briefly, this method finds edges using an

approximation of the derivative of the intensity value. It then terms ‘edges’ as locations in the comodulogram where the derivative exceeds a threshold value and is a local maximum. For more detail see (Vincent and Folorunso, 2009).

*Statistical Analysis*

To assess differences in behavior we used a one-sample t-test against the null hypothesis that the animals would spend equal time exploring each object. To assess differences in broadband subtracted power spectra as well as overall levels of broadband activity we employed unpaired two-sample t-tests. All t-tests were assessed at the $\alpha = 0.05$ level. In order to examine differences in PAC between behavioral conditions we performed a permutation based bootstrapping method designed to correct for multiple comparisons. At each point in the comodulogram space data from all individuals in each of the behavioral conditions to be analyzed was initially pooled, and subjects were then randomly assigned to two groups. A t-test was then performed and the value of the t statistic was saved. This procedure was repeated 500 times for each point in the comodulogram space creating a distribution of t values at each point. Next, we performed the comparison using the actual data groups, again by performing t-tests at each point in comodulogram space. Finally, we compared the t value from the actual comparison to the distribution of t values created using randomized groups at each point using a Z-test assessed at the $\alpha = 0.05$ level. This analysis was performed in MATLAB R2012b (Mathworks).

## **Results**

*Spatial Object Recognition Behavior*

The spatial object recognition task, along with its variants, have been well established as a rodent memory task used to assess hippocampal learning and memory processes in healthy rodents as well as disease models (Langston and Wood, 2009; Wimmer et al., 2012; Prince et al., 2014). Additionally, recent work in rats has described changes in *in vivo* single unit firing in hippocampal area CA1 during object recognition tasks (Larkin et al., 2014). The behavioral protocol we adopted was very similar to that presented in (Larkin et al., 2014), though the size of the box was scaled due to the fact that Larkin et al. used rats while we employ mice in our work (for details see *Methods,* for diagram see Figure 1A). Using this behavioral protocol subjects did not display an increased preference for exploring a similar object that had been spatially displaced (see Figure 1B, Novel location condition: NL. P=0.15). However, subjects did spend more time exploring a novel object that had been spatially displaced (Figure 1B, Novel object & location: NLO. P=0.012).

*Local Field Potential Power Spectrum Analysis*

In order to begin to determine the profile of the local field potential in hippocampal area CA1 across behavioral conditions, we computed the power spectrum of the local field potential during each of the three active behavioral conditions: familiarization (F), novel location (NL), and novel location & object (NLO). Power spectra across frequencies from 3 to 100 Hz are presented in Figure 2A-C, for individual animals as well as the group average in each behavioral condition. Before formally comparing local field potential recordings across behavioral conditions, we sought to separate the contributions of broadband activity from the activity of specific narrow band frequency ranges (e.g. theta:

4-12 Hz). In order to accomplish this, we logarithmically transformed both the axes of the power spectra (frequency and power) to linearize the data and subsequently fit each individual animal's power spectrum with a robust fit linear regression. After subtracting the robust fit line from the original power spectrum, the residual power describes the broadband corrected (or narrow band) power at each frequency (see Figure 2D-F). Additionally, the amount of broadband activity in each animal as well as condition was quantified by taking the mean of value of the robust fit line across frequencies. For more details on the broadband correction procedure see *Materials and Methods* and (Manning et al., 2009).

Next we sought to compare the narrowband and broadband activity across behavioral conditions. First we subtracted conditions with less novelty from those with more novelty (NL-Familiarization, NLO-Familiarization, NLO-NL) in order to determine the direction of any narrowband power changes in response to increasing novelty. We found a distinct increase in theta power (4-12 Hz) as well as a less pronounced increase in high gamma (70-100 Hz) in behavioral conditions with increasing novelty (see Figure 3A-C). In order to determine the significance of these observed differences, we performed unpaired two-sample t-tests comparing each possible pair of behavioral conditions assessed at an $\alpha = 0.05$ level. This revealed a significant effect of novelty in the theta range only when comparing NLO vs. NL conditions (see Figure 3F). Despite the fact the magnitude of the high gamma band difference was less pronounced it proved to be significant in both NLO vs. Familiarization and NLO vs. NL comparisons (see Figure 3E,F).

Additionally, we compared the amount of broadband activity in each behavioral condition. This comparison did not reveal any significant differences between behavioral conditions (data not shown).

*Single Electrode Phase Amplitude Coupling*

Recently, researchers studying neuronal oscillations have shown an increasing interest in the associations between different frequency bands in the local field potential (Lisman, 2005; Canolty et al., 2006; Tort et al., 2008; 2009; 2010). In particular, research starting with Bragin (Bragin et al., 1995) has shown an association between the phase of a low frequency signal in the theta frequency range and the amplitude of a higher frequency signal in the gamma frequency range. In an effort to measure the extent to which the phase of low frequency signals correlated with the amplitude of higher frequency signals we measured phase-amplitude coupling based on the methods of (Berman et al., 2012) and described in *Materials and Methods.* Computing phase-amplitude coupling at each possible pair of frequencies results in a comodulogram. We constructed comodulograms in this case by averaging across five minutes of data from each of the behavioral conditions (F, NL, and NLO).

First, we constructed comodulograms at each possible frequency pair using the data from a single electrode in hippocampal area CA1 (see Figure 4A-C). This revealed specific pairs of frequencies that had noteworthy phase-amplitude relations. Specifically, in all conditions the phase of 4 Hz activity influenced multiple higher frequencies, as did 8-10 Hz band activity. Next, we were interested in determining if there were any differences in PAC across behavioral conditions. In order to investigate this, we performed a non-parametric permutation based bootstrapping procedure to hypothesis test whether PAC varied significantly between two behavioral conditions at all possible pairs of frequencies (for details see *Materials and Methods*). We found no differences in PAC between behavioral conditions using data from a single electrode (Figure 4D-F).

*Dual Electrode Phase Amplitude Coupling*

In considering PAC comodulograms constructed from data from a single electrode we noted that some of the coupling observed may be due correlations in noise and therefore limit our ability to discriminate actual regions of interest where there is the 'signal' of a true relationship between the phase of a low frequency neuronal oscillation and the amplitude of a higher frequency neuronal oscillation. To alleviate this problem we computed comodulograms from data from two electrodes from the same tetrode. Data from one tetrode was used for the phase information of lower frequencies (3-14 Hz), while data from a separate electrode was used for the amplitude information of higher frequencies (15-100 Hz). As previously described for data from a single electrode, we used this approach to construct comodulograms for each of the behavioral conditions. This approach yielded similar results for the 4 Hz oscillation and its influence on multiple higher frequencies. However, in the 8-10 Hz band we were better able to resolve specific frequencies that had high PAC across behavioral conditions. Specifically, the phase of 8-10 Hz oscillations were associated with amplitude modulation in the 40 Hz range as well as the 80-90 Hz range (see Figure 5A-C). When we tested for differences between the behavioral conditions, we found just one point in comodulogram space (one pair of frequencies) that was significantly different between conditions again giving us reason to believe that PAC is not affected by behavioral condition (see Figure 5D-F).

*Dual Tetrode Phase Amplitude Coupling*

Upon observing a difference between PAC computed using a single electrode and PAC computed using separate electrodes for low frequencies and high frequencies, we wanted to determine if quantifying PAC using electrodes from two spatially distinct

tetrodes would further alleviate the noise problem we initially observed. We reanalyzed the data by computing PAC using one electrode for low frequency information (3-14 Hz) and selecting an electrode on a different tetrode for high frequency information (15-100 Hz). We computed PAC at all possible pairs of frequencies and for each behavioral session (see Figure 6A-C). Again prominent coupling can be observed between the 4 Hz oscillation and a range of higher frequencies. However, in the 8-10 Hz band the coupling became more spatially restricted to the 80-90 Hz region and to a lesser degree the 20 Hz band. Again we tested for differences between behavioral conditions and this time found a few pairs of frequencies that displayed significant differences between conditions. However, as the distribution of these differences is not consistent, it is more likely they are due to type I error and less likely to be true differences in PAC between behavioral conditions.

*Comparison of Phase Amplitude Coupling methods*

In order to quantify the differences between the methods of computing PAC (single electrode vs. two electrodes on the same tetrode vs. two electrodes on separate tetrodes) we sought to objectively count the edges in the average comodulograms (see Figures 4-6, A-C). Using Sobel's method of edge detection (for details see *Materials and Methods*) we sought to quantify the number of edges as more edges is expected to correlate with better ability to isolate regional areas of interest in the comodulogram, and inversely if the comodulogram does not contain regional differences we expected not to detect any edges. We detected more edges in both the methods employing two electrodes to compute PAC compared to a single electrode (see Table 1). This supports the notion that quantifying PAC using two electrodes will be more useful in detecting interactions between low and high frequency neuronal oscillations.

## Discussion

*Spatial Object Recognition Behavior*

We used spatial object recognition behavior as a way to pilot our *in vivo* recording methods as it provided a behavior that involved the hippocampus, the brain area we sought to record from in these initial experiments. We found that using the specific paradigm and parameters that we employed in these experiments our sham-operated animals were not able to discriminate between a familiar object in the same location as previously observed and a familiar object that had been spatially displaced. However, our sham-operated animals were able to discriminate between a familiar object in the same location as previously observed and a novel object positioned in a novel location. Interestingly, we observed a bimodal distribution of scores in the object recognition behavioral tasks. While some animals seemed to have learned the identity and location of the objects and were able to preserve that memory as indicated by scores around 0.7 or even higher on the Novelty Exploration metric, other animals were clearly not able to perform the task and scored very near or even slightly below 0.5. This was especially evident for the NL condition where the animals were exposed to two familiar objects, one having been spatially displaced. We hypothesize that this may be due to a lack of true familiarity with the objects. That is, the animals were not exposed to the objects long enough, and/or did not spend enough time exploring them to truly become familiar with them before the NL condition. Therefore in future experiments we will increase the time spent in the F condition, or simply repeat it once or more in order to provide more opportunity for the animals to become familiar with the objects. Additionally, we may

choose to reduce the size of the behavioral arena to encourage the animals to spend more time exploring the objects and less time exploring the arena itself.

*Spectral Analysis of Local Field Potentials*

In order to probe whether there were differences in neuronal oscillations in different behavioral conditions in the object recognition paradigm we calculated power-frequency spectra for each animal across a range of frequencies from 3-100 Hz. Next, in order to separate the contributions of broadband activity from specific narrow band activity we performed a regression-based method of broadband subtraction and computed residual power that was selectively attributable to narrow frequency bands. We found no differences in broadband activity between behavioral conditions, however we found that power in the theta and high gamma frequency bands increased as object novelty increased in the object recognition behavioral task. This is a very interesting result, but more crucial to the goals of the current project is the implementation of the methods of analysis exhibited in this section. We expect that further investigations into local field potential signatures of brain injury in the brain structures involved in working memory, including both the hippocampus and the medial prefrontal cortex, will reveal changes in both broadband activity and narrow band activity. It is critical then, that we can separate these two types of activity as they each have unique biological mechanisms. Broadband activity is characterized by voltage fluctuations across the entire spectrum of frequencies following a random-walk process, and is indicative of the general level of neuronal firing unlike true neuronal oscillatory behavior (Manning et al., 2009). Therefore, it will be critical to tease out which of these biological mechanisms may be responsible for both

electrophysiological and behavioral differences between brain-injured and sham-operated control animals.

*Phase-Amplitude Coupling*

To investigate interactions between different narrowband neuronal oscillations we quantified the strength of the correlation between the phase of a range of low frequency oscillations with the amplitude of higher frequency oscillations. This metric called Phase-Amplitude Coupling (PAC) is displayed in the comodulograms in Figures 4-6. We did not observe any consistent, interpretable differences in PAC across behavioral conditions. However, this does not dampen our enthusiasm for the applicability of PAC in our future experiments investigating neurophysiological differences between brain-injured animals and sham-operated controls. It is yet to be determined whether brain-injured animals will show differences between behavioral conditions or show differences in PAC when compared to sham-operated controls. We were able to observe interesting differences in comodulograms across different methods of quantifying PAC. These pilot analyses demonstrated that it will be most useful to quantify PAC using two separate electrodes for low and high frequencies. However, at least when both electrodes are in the same brain structure, there does not seem to be an advantage to using electrodes on separate tetrodes.

*Future Directions*

Future experiments will seek to determine the post-TBI changes that can be recorded in awake-behaving mice performing a memory task. We plan to record from both the hippocampus and the medial prefrontal cortex while animals perform a working memory task. We expect to see changes in oscillatory activity in both brain structures after TBI due to previous results in our lab and others using *ex vivo* physiology approaches. However, these new *in vivo* experiments will allow us to investigate two interesting aspects of these neuronal circuits for the first time. First, it will allow us to investigate the function/dysfunction of these circuits at the specific moment when a memory is being recalled, and second it allows us an opportunity to record from completely intact circuits to interrogate the critical interplay between these two memory structures. We believe that this approach will lead to insights not available in previous studies of experimental TBI and will greatly push forward the field's understanding of the circuit dysfunction suffered by TBI patients.

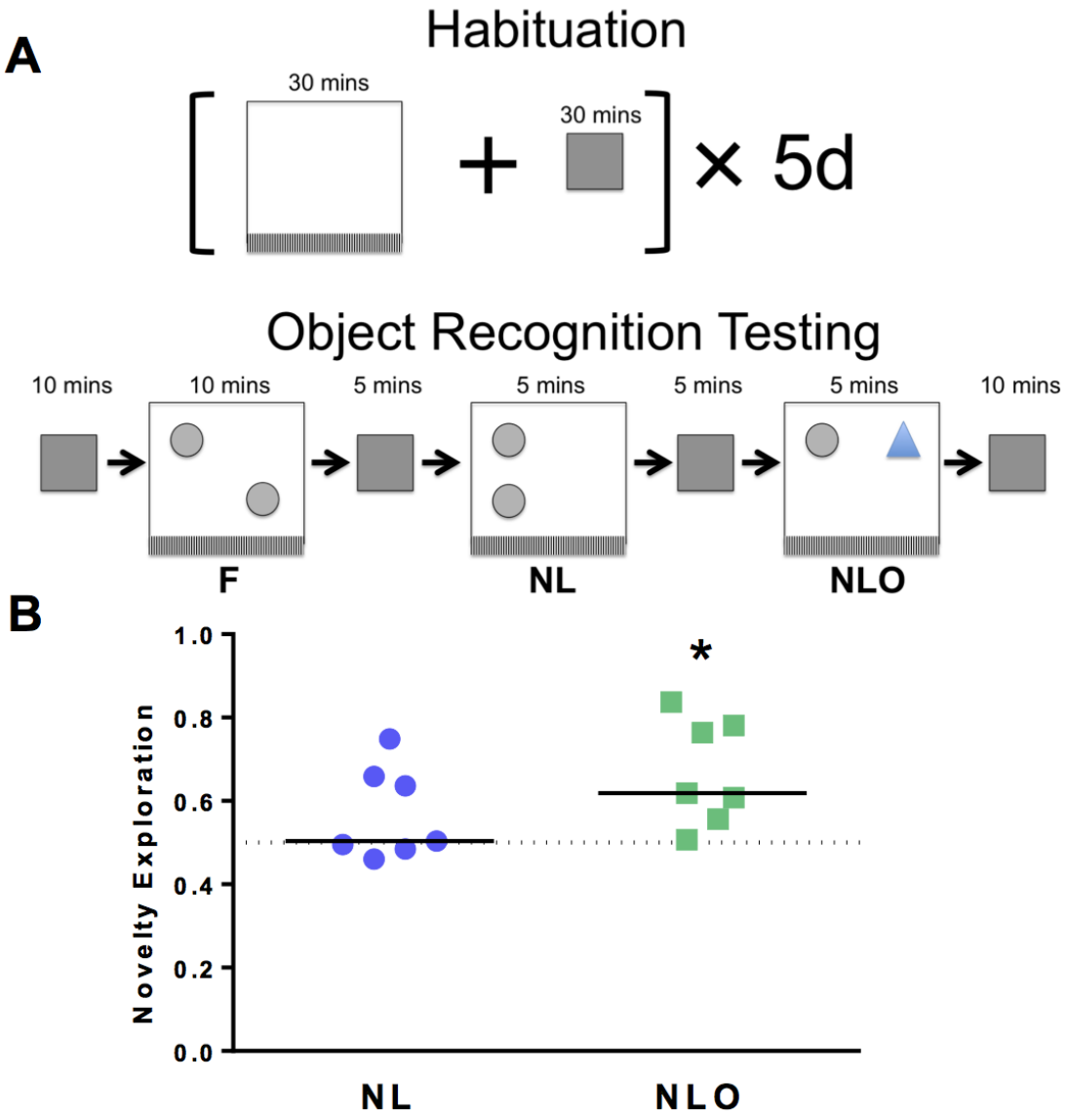


**Figure 1:** *Novel Location and Object Recognition Testing.* **A.** Behavioral paradigm. Mice were habituated for 5 consecutive days. Habituation sessions consisted of 30 minutes in the arena and 30 minutes in the rest box. On day 6 the object recognition testing session was performed. Object recognition testing consisted a ten-minute exposure to two identical objects in the arena (F), then a five-minute session where one of the objects was spatially displaced relative to the F session (NL), and finally a five-minute session where a novel object was introduced in a spatially displaced location relative to both the F and NL sessions (NLO). These testing sessions (F, NL, and NLO) were interleaved with session in the rest box, represented graphically by the small gray square. **B.** Novelty Exploration ratio. Novelty Exploration is the amount of time spent near the spatially displaced or spatially displaced and novel object divided by the total time spent near either object. In NL sessions Novelty Exploration was not significantly different than 0.5, while in NLO sessions Novelty Exploration was significantly greater than 0.5 (P=0.012).

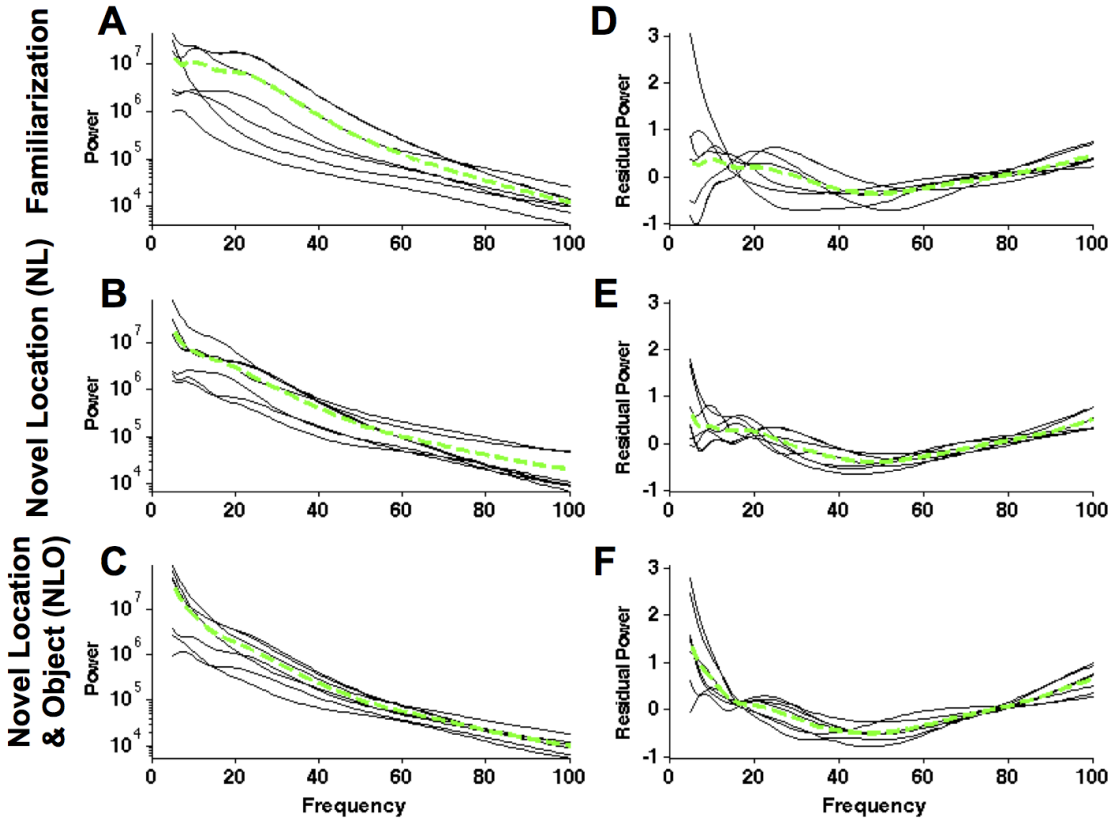


**Figure 2:** *Power spectra across behavioral sessions.* **A.** The power spectra from all animals (black lines) and averaged power spectra (green dashed line) during familiarization (F) sessions. **B.** Power spectra during novel location (NL) sessions. **C.** Power spectra during novel location and object (NLO) sessions. **D.** Broadband subtracted (residual) power spectra during F sessions. Residual power was computed after subtracting the broadband activity from the power spectra (for details see *Materials and Methods*). **E.** Broadband subtracted (residual) power spectra during NL sessions. **F.** Broadband subtracted (residual) power spectra during NLO sessions.

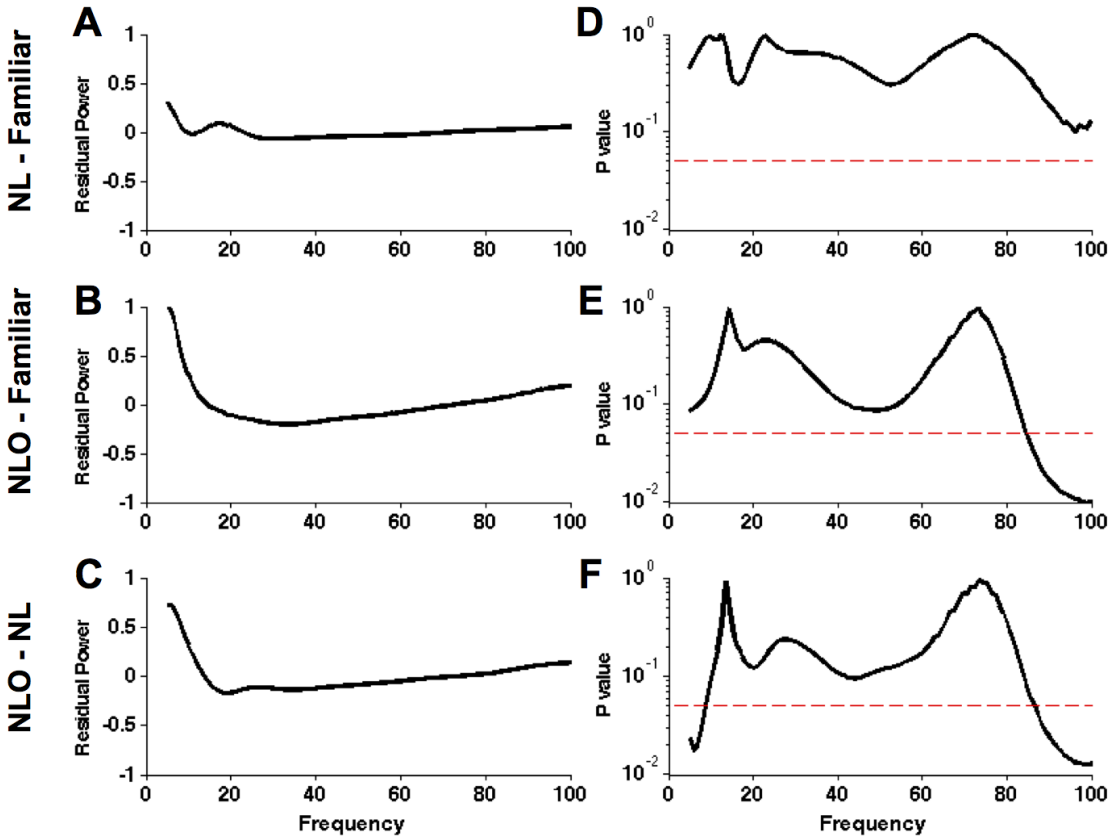


**Figure 3:** *Increasing Novelty correlates with Increases in Theta and High Gamma Power.* **A.** Residual power spectra resulting from subtracting Familiar residual power spectra (Fig. 2D) from NL residual power spectra (Fig. 2E). **B.** Residual power spectra resulting from subtracting Familiar residual power spectra (Fig. 2D) from NLO residual power spectra (Fig. 2F). Note positive values in the theta and high gamma ranges. **C.** Residual power spectra resulting from subtracting NL residual power spectra (Fig. 2E) from NLO residual power spectra (Fig. 2F). Note positive values in the theta and high gamma ranges. **D.** Individual t-tests were performed to assess the significance of non-zero residual power values in A. Red dashed line indicates P=.05 level. Note no significant differences in power spectra between NL and Familiar behavioral conditions. **E.** Same analysis and visualization as in D. However, note that high gamma is significantly increased in NLO condition compared to Familiar condition. **F.** Same analysis and visualization as in D and E. However, note that theta and high gamma are significantly increased in NLO condition compared to NL condition.

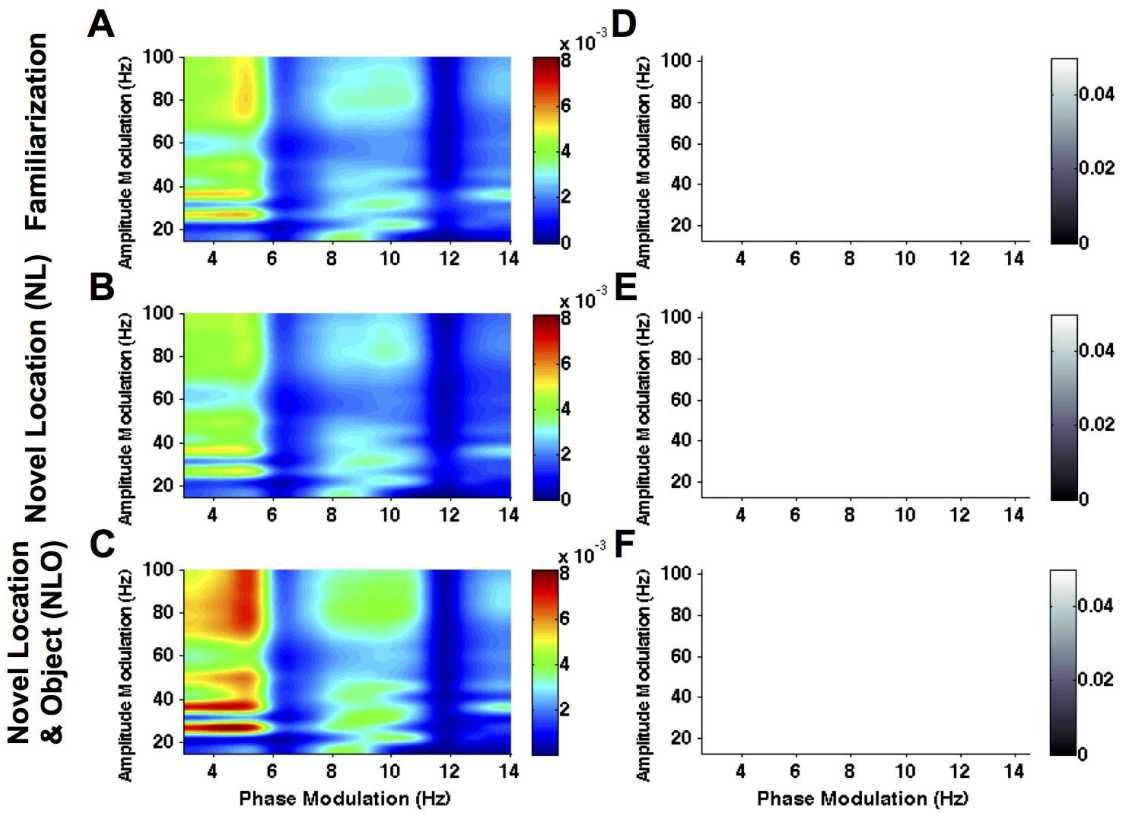


**Figure 4:** *Phase Amplitude Coupling on a Single Electrode.* **A.** Comodulogram from Familiarization behavioral sessions displaying modulation index from a single electrode in area CA1. Warmer colors indicates higher correlation between the phase of the lower frequencies (x-axis) and the amplitude of the higher frequencies (y-axis). **B.** Comodulogram from Novel Location (NL) behavioral sessions displaying modulation index from a single electrode in area CA1. **C.** Comodulogram from Novel Location and Object (NLO) behavioral sessions displaying modulation index from a single electrode in area CA1. **D.** A bootstrapping procedure was performed to assess the significance of any differences between PAC in NL and Familiarization behavioral conditions. Darker boxes indicate significant comparisons. The entirely white plot indicates that there were no significant differences in PAC between NL and Familiarization behavioral conditions. **E.** Same analysis as in D for NLO versus Familiarization behavioral conditions. The entirely white plot indicates that there were no significant differences in PAC between NLO and Familiarization behavioral conditions. **F.** Same analysis as in D and E for NLO versus NL behavioral conditions. The entirely white plot indicates that there were no significant differences in PAC between NLO and NL behavioral conditions.

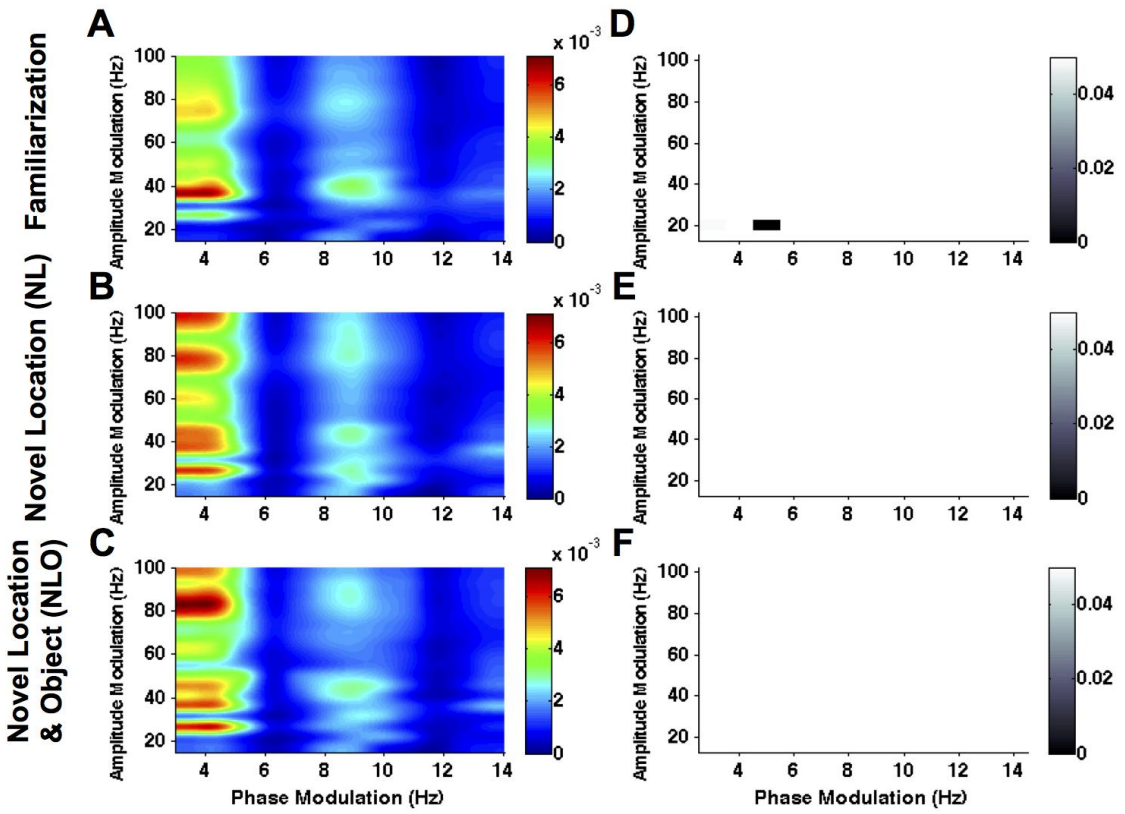


**Figure 5:** *Phase Amplitude Coupling on Two Electrodes From the Same Tetrode.* **A.** Comodulogram from Familiarization behavioral sessions displaying modulation index between two electrodes on the same tetrode in area CA1. The data from one electrode was used for lower frequencies (3-14 Hz) while data from the other electrode was used for higher frequencies (15-100 Hz). Warmer colors indicates higher correlation between the phase of the lower frequencies (x-axis) and the amplitude of the higher frequencies (y-axis). **B.** Comodulogram from Novel Location (NL) behavioral sessions displaying modulation index between two electrodes on the same tetrode in area CA1. **C.** Comodulogram from Novel Location and Object (NLO) behavioral sessions displaying modulation index between two electrodes on the same tetrode in area CA1. **D.** A bootstrapping procedure was performed to assess the significance of any differences between PAC in NL and Familiarization behavioral conditions. Darker boxes indicate significant comparisons. **E.** Same analysis as in D for NLO versus Familiarization behavioral conditions. The entirely white plot indicates that there were no significant differences in PAC between NLO and Familiarization behavioral conditions. **F.** Same analysis as in D and E for NLO versus NL behavioral conditions. The entirely white plot indicates that there were no significant differences in PAC between NLO and NL behavioral conditions.

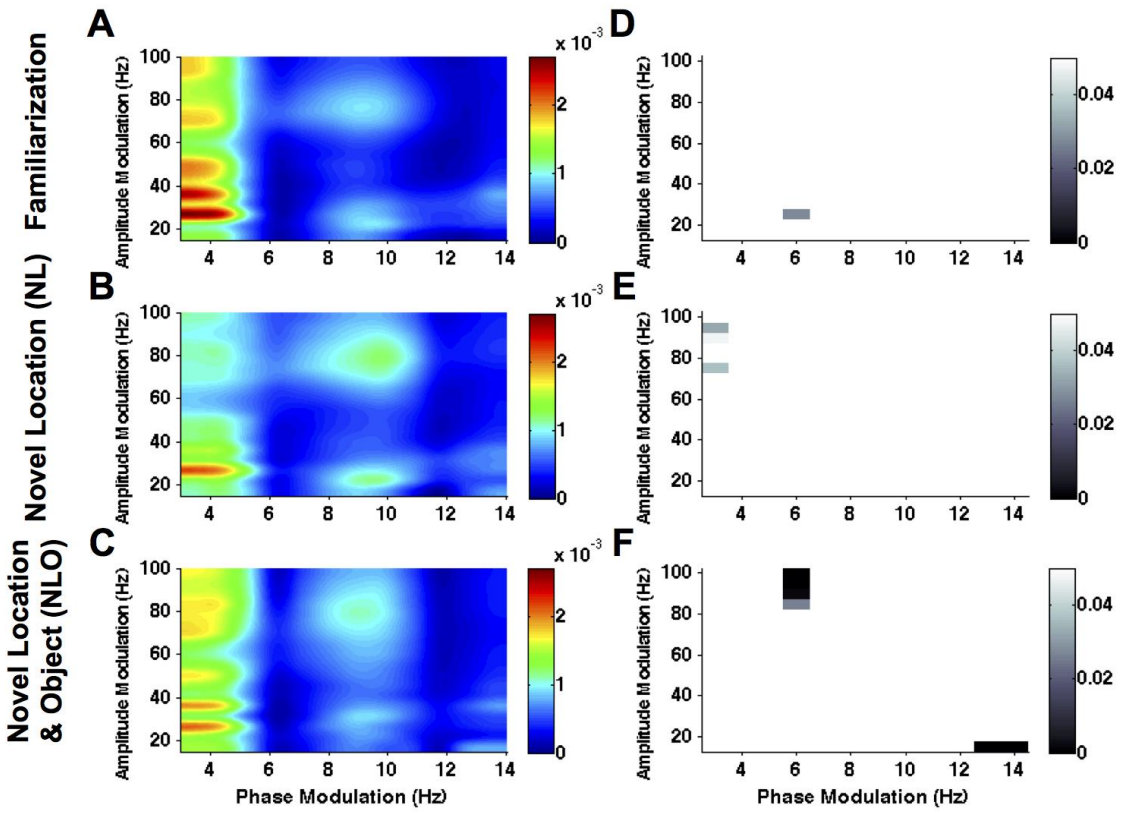


**Figure 6:** *Phase Amplitude Coupling on Two Electrodes From Different Tetrodes.* **A.** Comodulogram from Familiarization behavioral sessions displaying modulation index between two electrodes on different tetrodes in area CA1. The data from one electrode was used for lower frequencies (3-14 Hz) while data from the other electrode was used for higher frequencies (15-100 Hz). Warmer colors indicates higher correlation between the phase of the lower frequencies (x-axis) and the amplitude of the higher frequencies (y-axis). **B.** Comodulogram from Novel Location (NL) behavioral sessions displaying modulation index between two electrodes on different tetrodes in area CA1. **C.** Comodulogram from Novel Location and Object (NLO) behavioral sessions displaying modulation index between two electrodes on different tetrodes in area CA1. **D.** A bootstrapping procedure was performed to assess the significance of any differences between PAC in NL and Familiarization behavioral conditions. Darker boxes indicate significant comparisons. **E.** Same analysis as in D for NLO versus Familiarization behavioral conditions. **F.** Same analysis as in D and E for NLO versus NL behavioral conditions.

| | Familiarization | NL | NLO |
|---|---|---|---|
| Single electrode | 3 | 4 | 9 |
| Two electrodes/same electrode | 13 | 14 | 14 |
| Two electrodes/different electrode | 11 | 14 | 10 |

**Table 1:** *Edge detection differences across PAC methods.* The number of Sobel's edges in the comodulogram of each condition is quantified here. Both methods employing two electrodes are able to resolve more edges than PAC using a single electrode.

# CONCLUSIONS AND FUTURE DIRECTIONS

Chapter 2 details work demonstrating a sustained post-injury working memory impairment in the first week after LFPI. Additionally, the work details a shift in network excitability in the mPFC as assessed by extracellular field potentials recorded in brain slices from brain-injured and sham-operated mice. Subsequent experiments detail the changes in synaptic excitation and inhibition onto layer 2/3 and layer 5 neurons in the mPFC after LFPI. These experiments demonstrated an increase in net synaptic excitation onto layer 2/3 neurons, but no change to the synaptic input to layer 5 neurons. Interestingly, experiments probing the intrinsic excitability of layer 2/3 neurons revealed that these cells were less likely to fire after injury, as assessed by both action potential firing rates and action potential threshold. This post-injury change to intrinsic excitability is directionally opposed to the observed changes in the synaptic inputs to these cells after injury.

The experiments presented in Chapter 2 are the first to describe working memory impairments in the first week after LFPI. Additionally, the post-injury reduction in field excitatory postsynaptic potentials supports the hypothesis that E/I balance is disrupted after brain injury. Furthermore, this result is the first to demonstrate a decrease in network excitability in the mPFC after brain injury, supporting the notion that the prefrontal cortex contributes to observed memory impairments after brain injury. Finally, this work provides possible synaptic mechanisms that may begin to explain the mechanism behind the shift in network excitability. These investigations demonstrate that injury sensitivity in the mPFC is layer specific, much like the subregion specificity observed in the hippocampus after brain injury.

In chapter 3, I present a pilot study that lays the groundwork for future experiments probing post-injury memory circuit dysfunction that will employ *in vivo* recording methods to monitor brain activity from awake-behaving animals after LFPI. In the pilot study I demonstrate high quality recordings of local field potentials from the hippocampus of awake-behaving mice after they receive a sham surgery. Most importantly, I present a framework for data analysis of behavior and local field potentials. Additionally, I have developed software, written in MATLAB, which is used to automate data analysis of both behavioral and local field potential data. Using this software package I present comparisons between conditions of the behavioral experiment. These comparisons reveal increases in power of the theta band (6-12 Hz) as well as the high gamma band (70-100 Hz) in behavioral sessions where animals are subjected to novel objects and novel locations of objects. While previous work has investigated the role of the hippocampal oscillations in novelty detection, this result confirms that our recording and analysis methods can detect changes in electrophysiological measures that have previously been studied in similar behavioral experiments (O'Keefe, 1993; Jeewajee et al., 2008; Chang and Huerta, 2012).

From this pilot study we can draw conclusions of practical importance that will assist in the construction of future experiments. Chiefly, this pilot study has provided the knowledge base necessary to produce protocols for successfully recording of local field potentials during memory experiments. The details of these proposed future experiments are presented in the next section.

*Future Directions*

The behavioral experiments in chapter 2 demonstrate a post-injury working memory impairment in the delayed non-match to sample T-maze task. In these experiments the delay phase was a nominal zero seconds, however previous reports using the delayed non-match to sample T-maze task in rats have shown a delay dependent working memory deficit (Whiting and Hamm, 2006; Eakin and Miller, 2012). That is, the working memory impairment is only apparent as the delay phase is increased, making the task more difficult. Due to the small (but significant) effect seen in the experiments presented here, future work will examine the possibility of increasing the delay period to make the task more cognitively demanding. It is expected that this will increase the observed difference in memory performance between brain-injured mice and sham-operated controls.

The results presented in chapter 2 detail augmented excitatory synaptic input together with decreased inhibition onto layer 2/3 neurons, thereby producing a net increase in excitatory synaptic input following LFPI. In opposition to these changes, intrinsic excitability measures specifically firing rate and action potential threshold, were shifted in the opposite direction after LFPI, making layer 2/3 cells in slices derived from injured animals less likely to fire. Opposing alterations in synaptic transmission and intrinsic excitability have previously been described after LFPI, though not in the mPFC (Howard et al., 2007). It is possible that the alterations in intrinsic parameters may be due to a compensatory response of the layer 2/3 neurons in response to the observed net increase in excitatory input. This type of self-scaling or homeostatic response to changes in synaptic input has previously been described in the neocortex in response to experimental manipulation of synaptic input (Turrigiano, 2008; 2011). In light of the

results of chapter 2, it would be useful to show that specifically increasing excitatory input to mPFC layer 2/3 is sufficient to drive the observed alterations in intrinsic excitability. Furthermore, future experiments would determine whether specifically preventing the post-injury increase in excitatory input to the mPFC also prevents post-injury alterations in intrinsic excitability. This manipulation could be made a variety of ways, most notably silencing of the inputs to layer 2/3 using optogenetics or through the use of “chemogenetics” i.e., designer receptors exclusively activated by designer drugs (DREADDs) (Ferguson and Neumaier, 2012). However, it may be difficult to identify the specific inputs to layer 2/3 that have been altered by injury and thus difficult to genetically target them for experimental manipulation.

Additionally, future experiments should address the differential vulnerability to injury of layer 2/3 neurons and layer 5 neurons in the mPFC. There are two types of neurons within the mPFC that send excitatory projections to other regions. Layer 2/3 consists of only intratelencephalic (IT) neurons, which project to other cortical areas, while layer 5 contains both IT neurons and pyradmidal tract (PT) neurons which project to deeper brain structures (Molnár and Cheung, 2006; Shepherd, 2013; Dembrow and Johnston, 2014). It is possible that the layer specific vulnerability described in chapter 2 may indeed be a neuronal subtype specific vulnerability. That is, IT neurons may be more affected by brain injury than PT neurons. This hypothesis could be examined by recording from neurons of known subtype (IT or PT neurons), presumably after tagging these neurons with a fluorescent reporter preferentially expressed in one neuronal subtype.

It is possible that this presumed neuronal subtype specific vulnerability could be tied to the fact that IT neurons and PT neurons respond differentially to neuromodulators including dopamine and serotonin (Avesar and Gulledge, 2012; Seong and Carter, 2012). Further experiments could also examine the potential role of neuromodulators in the vulnerability of IT neurons, and could provide a possible route for reinstatement of E/I balance within the circuit through drug application of exogenous ligands that bind neuromodulator receptors.

Lastly, it is probable that the differential cohorts of intrinsic membrane channels, known to have a role in the distinct circuit function of IT and PT neurons, may provide a substrate for the increased action potential threshold and decreased firing rate of layer 2/3 neurons after injury (Dembrow et al., 2010; Kalmbach et al., 2013). Altering intrinsic properties of mPFC neurons has previously been shown to cause bi-directional changes in memory performance, and may be a biological mechanism causing the observed working memory impairment after LFPI (Wang et al., 2007; Thuault et al., 2013). In particular D-type potassium channels have been shown to play a regulatory role in homeostatic scaling of intrinsic excitability response to changes in synaptic input and may be upregulated after LFPI (Cudmore et al., 2010).

The pilot experiments presented in chapter 3 provide a plethora of future directions some of which I will offer here. Most concretely, these experiments have provided a basis for ongoing experiments within the Cohen lab that seek to determine the phase of memory (i.e. encoding, maintenance and/or retrieval) that is disrupted by the circuit changes that the lab and others have previously observed after LFPI (Witgen et al., 2005; Cole et al., 2010; Johnson et al., 2014). These ongoing experiments will vary the

time delay between the familiarization period and the testing period of the spatial object recognition test, which is equivalent to the NL condition presented in chapter 3. Similar to the pilot experiments presented here, the new experiments will feature *in vivo* recording of local field potentials during behavioral testing. However in upcoming experiments electrodes will be placed in both area CA1 and area CA3 of hippocampus. The experiments herein have provided data both on effective time delays and the amount of familiarization required to produce robust spatial object learning as well as best practices for Microdrive construction and implantation that are crucial to the ongoing study.

It is expected that further experiments will also include experiments to record from both area CA1 and mPFC simultaneously while animals perform the delayed non-match to sample task in the T-maze. This experiment would be designed to elucidate the *in vivo* relevance of the circuit alterations described in chapter 2. This experiment would also provide important information on the potential injury induced alterations in the relationship between the hippocampus and the mPFC, as measured by coherence and phase-amplitude relationships between the local field potentials of the two regions. Additionally, by using the T-maze this experiment would have the advantage of more precisely time-locking changes in the local field potential to observable, discrete behavioral responses allowing for more precision in the analysis of the neural data.

One specific electrophysiological signature of particular interest in the proposed CA1-mPFC dual recordings is gamma frequency (40-100 Hz) oscillations in the local field

potential. It has been proposed that neural activity in the gamma frequency band may play a role in coordinating activity between distant brain regions such as hippocampus and mPFC (Engel and Singer, 2001; Singer, 2009). Furthermore, increases in gamma oscillatory power in both the hippocampus and the frontal cortices have been shown to predict successful memory formation and retrieval in humans (Sederberg et al., 2006; 2007). Disordered gamma oscillations are also observed in other neurological syndromes, specifically schizophrenia and autism (Spencer et al., 2004; Light et al., 2006; Rojas et al., 2011). Translationally focused research in schizophrenia has worked to establish altered gamma oscillations as a endophenotype of the disease (Carlson et al., 2011; Hall et al., 2011; Kim et al., 2014; Rosen et al., 2015). This approach allows clinically focused research to work to assess possible biological mechanisms of the disease by measuring the signature of the endophenotype after manipulation of potential cellular or molecular substrates.

Further down the line, it would be relevant to record single-unit data from LFPI animals. While this has never been done before in mice, the Microdrives and tetrodes used in the pilot experiments in chapter 3 are fully capable of recording single-unit activity. Because one of the recent findings of the Cohen lab is not only a decrease in network excitability in CA1, but specifically a decrease in the evoked firing output of CA1 neurons after brain injury (Johnson et al., 2014). It would be useful to recapitulate this result *in vivo* by measuring CA1 unit firing. Similarly, it is expected that the lab would use both current the dietary therapy (Cole et al., 2010) as well as DREADD technology to show whether reinstating E/I balance through previously hypothesized mechanisms indeed restores *in vivo* output of area CA1.

*Translational implications*

The translational impact of this work rests on its potential as a building block for future studies. Perhaps the most interesting translational aspect of this work, and a major motivation for beginning studies measuring local field potentials, is the potential for local field potential recording to reveal an electrophysiological signature of brain injury that can be measured *in vivo* from both mice and humans. This putative electrophysiological signature of injury could be used as an endophenotype or biomarker. This would allow clinicians and researchers to better assess a patient's injury status after a potential TBI and also to assess whether a patient has completely recovered from a TBI before recommending they return to normal activity. Currently, diagnosis of mTBI and return to play guidelines are based on behavioral measures that are notoriously unreliable. An electrophysiological endophenotype would provide a more objective test of injury severity and recovery. Additionally, this electrophysiological signature could be measured in rodents while developing potential therapies as well as being measured during clinical trials of the therapies in TBI patients. An electrophysiological endophenotype would provide a more robust measure of the therapeutic profile of potential TBI drugs, allowing clinicians to more easily titrate dosage and determine efficacy of treatments in real time.

Given the continuing goal of the Cohen lab in producing dietary therapeutics to ameliorate the cognitive symptoms of brain injury, it is expected that the studies

presented here will provide the basis for future work assessing potential therapeutics. The Cohen lab is currently engaged in a clinical trial employing branched chain amino acids (BCAAs) as a post-injury therapy. These studies should provide a basis for further testing of BCAAs in a laboratory setting. First, investigations will be conducted to assess the effect of BCAA therapy on the layer specific alterations in the prefrontal cortex and associated memory behavior. Second, it is likely that the *in vivo* experiments proposed in the previous section will include groups of animals receiving BCAA therapy to determine whether BCAA therapy can restore putative electrophysiological signatures of injury.

# BIBLIOGRAPHY

Adams JH, Graham DI, Scott G, Parker LS, Doyle D (1980) Brain damage in fatal non-missile head injury. J Clin Pathol 33:1132–1145.

Aggleton JP, Hunt PR, Rawlins JN (1986) The effects of hippocampal lesions upon spatial and non-spatial tests of working memory. Behavioural Brain Research 19:133–146.

Arciniegas DB, Topkoff JL, Rojas DC, Sheeder J, Teale P, Young DA, Sandberg E, Reite ML, Adler LE (2001) Reduced hippocampal volume in association with p50 nonsuppression following traumatic brain injury. J Neuropsychiatry Clin Neurosci 13:213–221.

Atallah BV, Scanziani M (2009) Instantaneous Modulation of Gamma Oscillation Frequency by Balancing Excitation with Inhibition. Neuron 62:566–577.

Avesar D, Gulledge AT (2012) Selective serotonergic excitation of callosal projection neurons. Front Neural Circuits 6:12.

Axmacher N, Schmitz DP, Wagner T, Elger CE, Fell J (2008) Interactions between Medial Temporal Lobe, Prefrontal Cortex, and Inferior Temporal Regions during Visual Working Memory: A Combined Intracranial EEG and Functional Magnetic Resonance Imaging Study. Journal of Neuroscience 28:7304–7312.

Barker GRI, Warburton EC (2011) When Is the Hippocampus Involved in Recognition Memory? Journal of Neuroscience 31:10721–10731.

Benchenane K, Peyrache A, Khamassi M, Tierney PL, Gioanni Y, Battaglia FP, Wiener SI (2010) Coherent Theta Oscillations and Reorganization of Spike Timing in the

Hippocampal-Prefrontal Network upon Learning. Neuron 66:921–936.

Berman JI, McDaniel J, Liu S, Cornew L, Gaetz W, Roberts TPL, Edgar JC (2012) Variable Bandwidth Filtering for Improved Sensitivity of Cross-Frequency Coupling Metrics. Brain Connectivity 2:155–163.

Bigler ED, Andersob CV, Blatter DD (2002) Temporal lobe morphology in normal aging and traumatic brain injury. AJNR Am J Neuroradiol 23:255–266.

Bonislawski DP, Schwarzbach EP, Cohen AS (2007) Brain injury impairs dentate gyrus inhibitory efficacy. Neurobiology of Disease 25:163–169.

Bragin A, Jandó G, Nádasdy Z, Hetke J, Wise K, Buzsaki G (1995) Gamma (40-100 Hz) oscillation in the hippocampus of the behaving rat. J Neurosci 15:47–60.

Brito GN, Brito LS (1990) Septohippocampal system and the prelimbic sector of frontal cortex: a neuropsychological battery analysis in the rat. Behavioural Brain Research 36:127–146.

Canolty RT, Edwards E, Dalal SS, Soltani M, Nagarajan SS, Kirsch HE, Berger MS, Barbaro NM, Knight RT (2006) High Gamma Power Is Phase-Locked to Theta Oscillations in Human Neocortex. Science 313:1626–1628.

Carbonell WS, Maris DO, McCall T, Grady MS (1998) Adaptation of the fluid percussion injury model to the mouse. J Neurotrauma 15:217–229.

Carlson GC, Talbot K, Halene TB, Gandal MJ, Kazi HA, Schlosser L, Phung QH, Gur RE, Arnold SE, Siegel SJ (2011) Dysbindin-1 mutant mice implicate reduced fast-phasic inhibition

as a final common disease mechanism in schizophrenia. Proceedings of the National Academy of Sciences 108:E962–E970.

Cazalis F, Babikian T, Giza C, Copeland S, Hovda D, Asarnow RF (2011) Pivotal Role of Anterior Cingulate Cortex in Working Memory after Traumatic Brain Injury in Youth. Front Neur 1.

Centers for Disease Control and Prevention (2015) Report to Congress on Traumatic Brain Injury in the United States: Epidemiology and Rehabilitation. National Center for Injury Prevention and Control; Division of Unintentional Injury Prevention:1–72.

Chang EH, Huerta PT (2012) Neurophysiological correlates of object recognition in the dorsal subiculum. Front Behav Neurosci 6.

Chen Y, Mao H, Yang KH, Abel T, Meaney DF (2014) A modified controlled cortical impact technique to model mild traumatic brain injury mechanics in mice. Front Neur 5:100.

Cole JT, Mitala CM, Kundu S, Verma A, Elkind JA, Nissim I, Cohen AS (2010) Dietary branched chain amino acids ameliorate injury-induced cognitive impairment. Proceedings of the National Academy of Sciences 107:366–371.

Cortez SC, McIntosh TK, Noble LJ (1989) Experimental fluid percussion brain injury: vascular disruption and neuronal and glial alterations. Brain Research 482:271–282.

Courtney SM (2004) Attention and cognitive control as emergent properties of information representation in working memory. Cogn Affect Behav Neurosci 4:501–516.

Creed JA, DiLeonardi AM, Fox DP, Tessler AR, Raghupathi R (2011) Concussive Brain

Trauma in the Mouse Results in Acute Cognitive Deficits and Sustained Impairment of Axonal Function. J Neurotrauma 28:547–563.

Cudmore RH, Fronzaroli-Molinieres L, Giraud P, Debanne D (2010) Spike-Time Precision and Network Synchrony Are Controlled by the Homeostatic Regulation of the D-Type Potassium Current. Journal of Neuroscience 30:12885–12895.

Cui Y, Jin J, Zhang X, Xu H, Yang L, Du D, Zeng Q, Tsien JZ, Yu H, Cao X (2011) Forebrain NR2B Overexpression Facilitating the Prefrontal Cortex Long-Term Potentiation and Enhancing Working Memory Function in Mice Zhuang X, ed. PLoS ONE 6:e20312.

Curtis CE, D'Esposito M (2003) Persistent activity in the prefrontal cortex during working memory. Trends in Cognitive Sciences 7:415–423.

D'Ambrosio R, Maris DO, Grady MS, Winn HR, Janigro D (1998) Selective loss of hippocampal long-term potentiation, but not depression, following fluid percussion injury. Brain Research 786:64–79.

Dash PK, Moore AN, Moody MR, Treadwell R, Felix JL, Clifton GL (2004) Post-trauma administration of caffeine plus ethanol reduces contusion volume and improves working memory in rats. J Neurotrauma 21:1573–1583.

Dembrow N, Johnston D (2014) Subcircuit-specific neuromodulation in the prefrontal cortex. Front Neural Circuits 8:54.

Dembrow NC, Chitwood RA, Johnston D (2010) Projection-Specific Neuromodulation of Medial Prefrontal Cortex Neurons. Journal of Neuroscience 30:16922–16937.

Dixon CE, Lyeth BG, Povlishock JT, Findling RL, Hamm RJ, Marmarou A, Young HF, Hayes RL (1987) A fluid percussion model of experimental brain injury in the rat. J Neurosurg 67:110–119.

Doshi H, Wiseman N, Liu J, Wang W, Welch RD, O'Neil BJ, Zuk C, Wang X, Mika V, Szaflarski JP, Haacke EM, Kou Z (2015) Cerebral Hemodynamic Changes of Mild Traumatic Brain Injury at the Acute Stage Stamatakis EA, ed. PLoS ONE 10:e0118061.

Eakin K, Miller JP (2012) Mild Traumatic Brain Injury Is Associated with Impaired Hippocampal Spatiotemporal Representation in the Absence of Histological Changes. J Neurotrauma 29:1180–1187.

Engel AK, Singer W (2001) Temporal binding and the neural correlates of sensory awareness. Trends in Cognitive Sciences 5:16–25.

Ennaceur A, Aggleton JP (1997) The effects of neurotoxic lesions of the perirhinal cortex combined to fornix transection on object recognition memory in the rat. Behavioural Brain Research 88:181–193.

Faul M, Coronado V (2015) Epidemiology of traumatic brain injury. Handb Clin Neurol 127:3–13.

Fedor M, Berman RF, Muizelaar JP, Lyeth BG (2010) Hippocampal Theta Dysfunction after Lateral Fluid Percussion Injury. J Neurotrauma 27:1605–1615.

Ferguson SM, Neumaier JF (2012) npp2011179a. Neuropsychopharmacology 37:296–297.

Floresco SB, Seamans JK, Phillips AG (1997) Selective roles for hippocampal, prefrontal

cortical, and ventral striatal circuits in radial-arm maze tasks with or without a delay. J Neurosci 17:1880–1890.

Fujisawa S, Buzsáki G (2011) A 4 Hz Oscillation Adaptively Synchronizes Prefrontal, VTA, and Hippocampal Activities. Neuron 72:153–165.

Gilbert P (2004) Memory for objects and their locations: The role of the hippocampus in retention of object–place associations. Neurobiology of Learning and Memory 81:39–45.

Goldman-Rakic PS (1995) Cellular basis of working memory. Neuron 14:477–485.

Gordon JA (2011) Oscillations and hippocampal–prefrontal synchrony. Current Opinion in Neurobiology 21:486–491.

Gorman LK, Shook BL, Becker DP (1993) Traumatic brain injury produces impairments in long-term and recent memory. Brain Research 614:29–36.

Grady MS (1994) Anesthetic Management of Acute Head Injury (Arthur L, ed). Mcgraw-Hill.

Hall MH, Taylor G, Sham P, Schulze K, Rijsdijk F, Picchioni M, Toulopoulou T, Ettinger U, Bramon E, Murray RM, Salisbury DF (2011) The Early Auditory Gamma-Band Response Is Heritable and a Putative Endophenotype of Schizophrenia. Schizophrenia Bulletin 37:778–787.

Hearing M, Kotecki L, de Velasco EMF, Fajardo-Serrano A, Chung HJ, Luján R, Wickman K (2013) Repeated Cocaine Weakens GABA-Girk Signaling in Layer 5/6 Pyramidal Neurons in the Prelimbic Cortex. Neuron 80:159–170.

Hicks RR, Smith DH, Lowenstein DH, Saint Marie R, McIntosh TK (1993) Mild experimental brain injury in the rat induces cognitive deficits associated with regional neuronal loss in the hippocampus. J Neurotrauma 10:405–414.

Hoskison MM, Moore AN, Hu B, Orsi S, Kobori N, Dash PK (2009) Persistent working memory dysfunction following traumatic brain injury: Evidence for a time-dependent mechanism. Neuroscience 159:483–491.

Howard AL, Neu A, Morgan RJ, Echegoyen JC, Soltesz I (2007) Opposing Modifications in Intrinsic Currents and Synaptic Inputs in Post-Traumatic Mossy Cells: Evidence for Single-Cell Homeostasis in a Hyperexcitable Network. Journal of Neurophysiology 97:2394–2409.

Huang Y-Y, Simpson E, Kellendonk C, Kandel ER (2004) Genetic evidence for the bidirectional modulation of synaptic plasticity in the prefrontal cortex by D1 receptors. Proc Natl Acad Sci USA 101:3236–3241.

Izaki Y, Maruki K, Hori K, Nomura M (2001) Effects of rat medial prefrontal cortex temporal inactivation on a delayed alternation task. Neuroscience Letters 315:129–132.

Jay TM, Thierry A-M, Wiklund L, Glowinski J (1992) Excitatory Amino Acid Pathway from the Hippocampus to the Prefrontal Cortex. Contribution of AMPA Receptors in Hippocampo-prefrontal Cortex Transmission. Eur J Neurosci 4:1285–1295.

Jay TM, Witter MP (1991) Distribution of hippocampal CA1 and subicular efferents in the prefrontal cortex of the rat studied by means of anterograde transport of Phaseolus vulgaris-leucoagglutinin. J Comp Neurol 313:574–586.

Jeewajee A, Lever C, Burton S, O'Keefe J, Burgess N (2008) Environmental novelty is signaled by reduction of the hippocampal theta frequency. Hippocampus 18:340–348.

Johnson BN, Palmer CP, Bourgeois EB, Elkind JA, Putnam BJ, Cohen AS (2014) Augmented Inhibition from Cannabinoid-Sensitive Interneurons Diminishes CA1 Output after Traumatic Brain Injury. Front Cell Neurosci 8:435.

Jones MW, Wilson MA (2005a) Theta Rhythms Coordinate Hippocampal–Prefrontal Interactions in a Spatial Memory Task. Plos Biol 3:e402.

Jones MW, Wilson MA (2005b) Phase precession of medial prefrontal cortical activity relative to the hippocampal theta rhythm. Hippocampus 15:867–873.

Kalmbach BE, Chitwood RA, Dembrow NC, Johnston D (2013) Dendritic Generation of mGluR-Mediated Slow Afterdepolarization in Layer 5 Neurons of Prefrontal Cortex. Journal of Neuroscience 33:13518–13532.

Kellendonk C, Simpson EH, Polan HJ, Malleret G, Vronskaya S, Winiger V, Moore H, Kandel ER (2006) Transient and Selective Overexpression of Dopamine D2 Receptors in the Striatum Causes Persistent Abnormalities in Prefrontal Cortex Functioning. Neuron 49:603–615.

Kim S-W, Seo M, Kim D-S, Kang M, Kim Y-S, Koh H-Y, Shin H-S (2014) Knockdown of phospholipase C-β1 in the medial prefrontal cortex of male mice impairs working memory among multiple schizophrenia endophenotypes. J Psychiatry Neurosci 39:130285.

Kobori N (2006) Reversal of Brain Injury-Induced Prefrontal Glutamic Acid Decarboxylase

Expression and Working Memory Deficits by D1 Receptor Antagonism. Journal of Neuroscience 26:4236–4246.

Korotkova T, Fuchs EC, Ponomarenko A, Engelhardt von J, Monyer H (2010) NMDA Receptor Ablation on Parvalbumin-Positive Interneurons Impairs Hippocampal Synchrony, Spatial Representations, and Working Memory. Neuron 68:557–569.

Kovner R, Stamm JS (1972) Disruption of short-term visual memory by electrical stimulation of inferotemporal cortex in the monkey. J Comp Physiol Psychol 81:163–172.

Kritzer MF, Goldman-Rakic PS (1995) Intrinsic circuit organization of the major layers and sublayers of the dorsolateral prefrontal cortex in the rhesus monkey. J Comp Neurol 359:131–143.

Laker SR (2011) Epidemiology of Concussion and Mild Traumatic Brain Injury. PMRJ 3:S354–S358.

Langston RF, Wood ER (2009) Associative recognition and the hippocampus: Differential effects of hippocampal lesions on object-place, object-context and object-place-context memory. Hippocampus 20:1139–1153.

Larkin MC, Lykken C, Tye LD, Wickelgren JG, Frank LM (2014) Hippocampal output area CA1 broadcasts a generalized novelty signal during an object-place recognition task. Hippocampus 24:773–783.

Lee DJ, Gurkoff GG, Izadi A, Berman RF, Ekstrom AD, Muizelaar JP, Lyeth BG, Shahlaie K (2013) Medial Septal Nucleus Theta Frequency Deep Brain Stimulation Improves

Spatial Working Memory after Traumatic Brain Injury. J Neurotrauma 30:131–139.

Lee I, Kesner RP (2003) Time-dependent relationship between the dorsal hippocampus and the prefrontal cortex in spatial memory. Journal of Neuroscience 23:1517–1523.

Lee J, Chung C, Ha S, Lee D, Kim D-Y, Kim H, Kim E (2015) Shank3-mutant mice lacking exon 9 show altered excitation/inhibition balance, enhanced rearing, and spatial memory deficit. Front Cell Neurosci 9.

Lewelt W, Jenkins LW, Miller JD (1982) Effects of experimental fluid-percussion injury of the brain on cerebrovascular reactivity of hypoxia and to hypercapnia. J Neurosurg 56:332–338.

Lewelt W, Jenkins LW, Miller JD (2009) Autoregulation of cerebral blood flow after experimental fluid percussion injury of the brain. J Neurosurg 53:500–511.

Lifshitz J, Kelley BJ, Povlishock JT (2007) Perisomatic thalamic axotomy after diffuse traumatic brain injury is associated with atrophy rather than cell death. J Neuropathol Exp Neurol 66:218–229.

Light GA, Hsu JL, Hsieh MH, Meyer-Gomes K, Sprock J, Swerdlow NR, Braff DL (2006) Gamma Band Oscillations Reveal Neural Network Cortical Coherence Dysfunction in Schizophrenia Patients. Biological Psychiatry 60:1231–1240.

Lishman WA (1968) Brain damage in relation to psychiatric disability after head injury. Br J Psychiatry 114:373–410.

Lisman J (2005) The theta/gamma discrete phase code occuring during the hippocampal

phase precession may be a more general brain coding scheme. Hippocampus 15:913–922.

Lyeth BG, Jenkins LW, Hamm RJ, Dixon CE, Phillips LL, Clifton GL, Young HF, Hayes RL (1990) Prolonged memory impairment in the absence of hippocampal cell death following traumatic brain injury in the rat. Brain Research 526:249–258.

Manning JR, Jacobs J, Kahana MJ (2009) Response to Miller. Journal of Neuroscience 29:13613–13620.

Markowitsch HJ, Calabrese P, Liess J, Haupts M, Durwen HF, Gehlen W (1993) Retrograde amnesia after traumatic injury of the fronto-temporal cortex. J Neurol Neurosurg Psychiatr 56:988–992.

Marquez de la Plata CD, Garces J, Shokri Kojori E, Grinnan J, Krishnan K, Pidikiti R, Spence J, Devous MD, Moore C, McColl R, Madden C, Diaz-Arrastia R (2011) Deficits in functional connectivity of hippocampal and frontal lobe circuits after traumatic axonal injury. Arch Neurol 68:74–84.

McAllister TW (1992) Neuropsychiatric sequelae of head injuries. Psychiatr Clin North Am 15:395–413.

McAllister TW, Flashman LA, McDonald BC, Saykin AJ (2006) Mechanisms of working memory dysfunction after mild and moderate TBI: evidence from functional MRI and neurogenetics. J Neurotrauma 23:1450–1467.

McAllister TW, Sparling MB, Flashman LA, Guerin SJ, Mamourian AC, Saykin AJ (2001) Differential Working Memory Load Effects after Mild Traumatic Brain Injury.

NeuroImage 14:1004–1012.

McHugh T, Laforce R, Gallagher P, Quinn S, Diggle P, Buchanan L (2006) Natural history of the long-term cognitive, affective, and physical sequelae of mild traumatic brain injury. Brain Cogn 60:209–211.

McIntosh TK, Noble L, Andrews B, Faden AI (1987) Traumatic brain injury in the rat: characterization of a midline fluid-percussion model. Cent Nerv Syst Trauma 4:119–134.

McIntosh TK, Vink R, Noble L, Yamakami I, Fernyak S, Soares H, Faden AL (1989) Traumatic brain injury in the rat: characterization of a lateral fluid-percussion model. Neuroscience 28:233–244.

Medicine ACOR (1993) Definition of mild traumatic brain injury. J Head Trauma Rehabil 8:86–87.

Milman A, Rosenberg A, Weizman R, Pick CG (2005) Mild traumatic brain injury induces persistent cognitive deficits and behavioral disturbances in mice. J Neurotrauma 22:1003–1010.

Molnár Z, Cheung AFP (2006) Towards the classification of subpopulations of layer V pyramidal projection neurons. Neuroscience Research 55:105–115.

Morehead M, Bartus RT, Dean RL, Miotke JA, Murphy S, Sall J, Goldman H (1994) Histopathologic consequences of moderate concussion in an animal model: correlations with duration of unconsciousness. J Neurotrauma 11:657–667.

Morishima M, Kawaguchi Y (2006) Recurrent connection patterns of corticostriatal pyramidal cells in frontal cortex. Journal of Neuroscience 26:4394–4405.

Moro N, Ghavim SS, Hovda DA, Sutton RL (2011) Delayed sodium pyruvate treatment improves working memory following experimental traumatic brain injury. Neuroscience Letters 491:158–162.

Mumby DG (2001) Perspectives on object-recognition memory following hippocampal damage: lessons from studies in rats. Behavioural Brain Research 127:159–181.

Munyon C, Eakin KC, Sweet JA, Miller JP (2014) Decreased bursting and novel object-specific cell firing in the hippocampus after mild traumatic brain injury. Brain Research 1582:220–226.

O'Keefe J (1993) Hippocampus, theta, and spatial memory. Current Opinion in Neurobiology 3:917–924.

Oliveira AMM, Hawk JD, Abel T, Havekes R (2010) Post-training reversible inactivation of the hippocampus enhances novel object recognition memory. Learning & Memory 17:155–160.

Olton DS, Wenk GL, Church RM, Meck WH (1988) Attention and the frontal cortex as examined by simultaneous temporal processing. Neuropsychologia 26:307–318.

Palacios EM, Sala-Llonch R, Junque C, Roig T, Tormos JM, Bargallo N, Vendrell P (2012) White matter integrity related to functional working memory networks in traumatic brain injury. Neurology 78:852–860.

Parent MA, Wang L, Su J, Netoff T, Yuan LL (2010) Identification of the Hippocampal Input to Medial Prefrontal Cortex In Vitro. Cerebral Cortex 20:393–403.

Park DC, Welsh RC, Marshuetz C, Gutchess AH, Mikels J, Polk TA, Noll DC, Taylor SF (2003) Working memory for complex scenes: age differences in frontal and hippocampal activations. J Cogn Neurosci 15:1122–1134.

Paxinos G, Franklin K (2004) The Mouse Brain in Stereotaxic Coordinates. Gulf Professional Publishing.

Petersson KM, Gisselgård J, Gretzer M, Ingvar M (2006) Interaction between a verbal working memory network and the medial temporal lobe. NeuroImage 33:1207–1217.

Plenger P, Krishnan K, Cloud M, Bosworth C, Qualls D, Marquez de la Plata C (2015) fNIRS-based investigation of the Stroop task after TBI. Brain Imaging and Behavior.

Prince T-M, Wimmer M, Choi J, Havekes R, Aton S, Abel T (2014) Neurobiology of Learning and Memory. Neurobiology of Learning and Memory 109:122–130.

Ranganath C, Cohen MX, Brozinsky CJ (2005) Working memory maintenance contributes to long-term memory formation: neural and behavioral evidence. J Cogn Neurosci 17:994–1010.

Ranganath C, D'Esposito M (2001) Medial temporal lobe activity associated with active maintenance of novel information. Neuron 31:865–873.

Rassovsky Y, Levi Y, Agranov E, Sela-Kaufman M, Sverdlik A, Vakil E (2015) Predicting long-term outcome following traumatic brain injury (TBI). Journal of Clinical and

Experimental Neuropsychology:1–13.

Riggio S (2010) Traumatic Brain Injury and Its Neurobehavioral Sequelae. Psychiatric Clinics of North America 33:807–819.

Rissman J, Gazzaley A, D'Esposito M (2008) Dynamic Adjustments in Prefrontal, Hippocampal, and Inferior Temporal Interactions with Increasing Visual Working Memory Load. Cerebral Cortex 18:1618–1629.

Rojas DC, Teale PD, Maharajh K, Kronberg E, Youngpeter K, Wilson LB, Wallace A, Hepburn S (2011) Transient and steady-state auditory gamma-band responses in first-degree relatives of people with autism spectrum disorder. Mol Autism 2:11.

Rosen AM, Spellman T, Gordon JA (2015) Electrophysiological Endophenotypes in Rodent Models of Schizophrenia and Psychosis. Biological Psychiatry:1–9.

Ross ST, Soltesz I (2000) Selective depolarization of interneurons in the early posttraumatic dentate gyrus: involvement of the Na(+)/K(+)-ATPase. Journal of Neurophysiology 83:2916–2930.

Rutland-Brown W, Langlois JA, Thomas KE, Xi YL (2006) Incidence of traumatic brain injury in the United States, 2003. J Head Trauma Rehabil 21:544–548.

Santhakumar V, Bender R, Frotscher M, Ross ST, Hollrigel GS, Toth Z, Soltesz I (2000) Granule cell hyperexcitability in the early post-traumatic rat dentate gyrus: the “irritable mossy cell” hypothesis. The Journal of Physiology 524 Pt 1:117–134.

Santhakumar V, Ratzliff ADH, Jeng J, Toth Z, Soltesz I (2002) Long-term hyperexcitability in

the hippocampus after experimental head trauma. Ann Neurol 50:708–717.

Sánchez-Carrión R, Gómez PV, Junqué C, Fernández-Espejo D, Falcon C, Bargalló N, Roig-Rovira T, Enseñat-Cantallops A, Bernabeu M (2008) Frontal Hypoactivation on Functional Magnetic Resonance Imaging in Working Memory after Severe Diffuse Traumatic Brain Injury. J Neurotrauma 25:479–494.

Schon K, Hasselmo ME, LoPresti ML, Tricarico MD, Stern CE (2004) Persistence of Parahippocampal Representation in the Absence of Stimulus Input Enhances Long-Term Encoding: A Functional Magnetic Resonance Imaging Study of Subsequent Memory after a Delayed Match-to-Sample Task. Journal of Neuroscience 24:11088–11097.

Schwabe K, Enkel T, Klein S, Schütte M, Koch M (2004) Effects of neonatal lesions of the medial prefrontal cortex on adult rat behaviour. Behavioural Brain Research 153:21–34.

Schwarzbach E, Bonislawski DP, Xiong G, Cohen AS (2006) Mechanisms underlying the inability to induce area CA1 LTP in the mouse after traumatic brain injury. Hippocampus 16:541–550.

Scoville WB, Milner B (1957) Loss of recent memory after bilateral hippocampal lesions. J Neurol Neurosurg Psychiatr 20:11–21.

Sederberg PB, Schulze-Bonhage A, Madsen JR, Bromfield EB, Litt B, Brandt A, Kahana MJ (2007) Gamma Oscillations Distinguish True From False Memories. Psychological Science 18:927–932.

Sederberg PB, Schulze-Bonhage A, Madsen JR, Bromfield EB, McCarthy DC, Brandt A, Tully MS, Kahana MJ (2006) Hippocampal and Neocortical Gamma Oscillations Predict Memory Formation in Humans. Cerebral Cortex 17:1190–1196.

Seong HJ, Carter AG (2012) D1 Receptor Modulation of Action Potential Firing in a Subpopulation of Layer 5 Pyramidal Neurons in the Prefrontal Cortex. Journal of Neuroscience 32:10516–10521.

Shepherd GMG (2013) Corticostriatal connectivity and its role in disease. Nat Rev Neurosci 14:1–14.

Siapas AG, Lubenov EV, Wilson MA (2005) Prefrontal Phase Locking to Hippocampal Theta Oscillations. Neuron 46:141–151.

Sigurdsson T, Stark KL, Karayiorgou M, Gogos JA, Gordon JA (2010) Impaired hippocampal–prefrontal synchrony in a genetic mouse model of schizophrenia. Nature 464:763–767.

Singer W (2009) Distributed processing and temporal codes in neuronal networks. Cogn Neurodyn 3:189–196.

Skelton RW, Bukach CM, Laurance HE, Thomas KGF, Jacobs JW (2000) Humans With Traumatic Brain Injuries Show Place-Learning Deficits in Computer-Generated Virtual Space. Journal of Clinical and Experimental Neuropsychology (Neuropsychology, Development and Cognition: Section A) 22:157–175.

Slovarp L, Azuma T, LaPointe L (2012) The effect of traumatic brain injury on sustained attention and working memory. Brain Inj 26:48–57.

Smith DH, Okiyama K, Thomas MJ, Claussen B, McIntosh TK (1991) Evaluation of memory dysfunction following experimental brain injury using the Morris water maze. J Neurotrauma 8:259–269.

Spencer K (2009) The functional consequences of cortical circuit abnormalities on gamma oscillations in schizophrenia: insights from computational modeling. Front Hum Neurosci 3.

Spencer KM, Nestor PG, Perlmutter R, Niznikiewicz MA, Klump MC, Frumin M, Shenton ME, McCarley RW (2004) Neural synchrony indexes disordered perception and cognition in schizophrenia. Proc Natl Acad Sci USA 101:17288–17293.

Squire LR, Stark CEL, Clark RE (2004) The Medial Temporal Lobe. Annu Rev Neurosci 27:279–306.

Squire LR, Zola-Morgan S (1991) The medial temporal lobe memory system. Science 253:1380–1386.

Stuss DT (2003) Staying on the job: the frontal lobes control individual performance variability. Brain 126:2363–2380.

Stuss DT (2011) Traumatic brain injury. Current Opinion in Neurology 24:584–589.

Stuss DT, Ely P, Hugenholtz H, Richard MT, LaRochelle S, Poirier CA, Bell I (1985) Subtle neuropsychological deficits in patients with good recovery after closed head injury. Neurosurgery 17:41–47.

Tate DF, Bigler ED (2000) Fornix and Hippocampal Atrophy in Traumatic Brain Injury.

Learning & Memory 7:442–446.

Thierry AM, Gioanni Y, Dégénétais E, Glowinski J (2000) Hippocampo-prefrontal cortex pathway: anatomical and electrophysiological characteristics. Hippocampus 10:411–419.

Thomas GJ, Spafford PS (1984) Deficits for representational memory induced by septal and cortical lesions (singly and combined) in rats. Behavioral Neuroscience 98:394–404.

Thompson HJ, Lifshitz J, Marklund N, Grady MS, Graham DI, Hovda DA, McIntosh TK (2005) Lateral fluid percussion brain injury: a 15-year review and evaluation. J Neurotrauma 22:42–75.

Thuault SJ, Malleret G, Constantinople CM, Nicholls R, Chen I, Zhu J, Panteleyev A, Vronskaya S, Nolan MF, Bruno R, Siegelbaum SA, Kandel ER (2013) Prefrontal Cortex HCN1 Channels Enable Intrinsic Persistent Neural Firing and Executive Memory Function. Journal of Neuroscience 33:13583–13599.

Tong KA, Ashwal S, Holshouser BA, Nickerson JP, Wall CJ, Shutter LA, Osterdock RJ, Haacke EM, Kido D (2004) Diffuse axonal injury in children: Clinical correlation with hemorrhagic lesions. Ann Neurol 56:36–50.

Tort ABL, Komorowski R, Eichenbaum H, Kopell N (2010) Measuring Phase-Amplitude Coupling Between Neuronal Oscillations of Different Frequencies. Journal of Neurophysiology 104:1195–1210.

Tort ABL, Komorowski RW, Manns JR, Kopell NJ, Eichenbaum H (2009) Theta-gamma coupling increases during the learning of item-context associations. Proceedings of the

National Academy of Sciences 106:20942–20947.

Tort ABL, Kramer MA, Thorn C, Gibson DJ, Kubota Y, Graybiel AM, Kopell NJ (2008) Dynamic cross-frequency couplings of local field potential oscillations in rat striatum and hippocampus during performance of a T-maze task. Proceedings of the National Academy of Sciences 105:20517–20522.

Toth Z, Hollrigel GS, Gorcs T, Soltesz I (1997) Instantaneous perturbation of dentate interneuronal networks by a pressure wave-transient delivered to the neocortex. J Neurosci 17:8106–8117.

Touzani K, Puthanveettil SV, Kandel ER (2007) Consolidation of learning strategies during spatial working memory task requires protein synthesis in the prefrontal cortex. Proc Natl Acad Sci USA 104:5632–5637.

Tran LD, Lifshitz J, Witgen BM, Schwarzbach E, Cohen AS, Grady MS (2006) Response of the contralateral hippocampus to lateral fluid percussion brain injury. J Neurotrauma 23:1330–1342.

Turrigiano G (2011) Too Many Cooks? Intrinsic and Synaptic Homeostatic Mechanisms in Cortical Circuit Refinement. Annu Rev Neurosci 34:89–103.

Turrigiano GG (2008) The Self-Tuning Neuron: Synaptic Scaling of Excitatory Synapses. Cell 135:422–435.

Uhl F, Lang W, Lindinger G, Deecke L (1990) Elaborative strategies in word pair learning--DC-potential correlates of differential frontal and temporal lobe involvement. Neuropsychologia 28:707–717.

Umile EM, Sandel ME, Alavi A, Terry CM, Plotkin RC (2002) Dynamic imaging in mild traumatic brain injury: Support for the theory of medial temporal vulnerability. Archives of Physical Medicine and Rehabilitation 83:1506–1513.

Vincent OR, Folorunso O (2009) A descriptive algorithm for sobel image edge detection. Proceedings of Informing Science & IT Education Conference InSITE.

Wang F, Zhu J, Zhu H, Zhang Q, Lin Z, Hu H (2011) Bidirectional Control of Social Hierarchy by Synaptic Efficacy in Medial Prefrontal Cortex. Science 334:693–697.

Wang G-W, Cai J-X (2006) Disconnection of the hippocampal–prefrontal cortical circuits impairs spatial working memory performance in rats. Behavioural Brain Research 175:329–336.

Wang M, Ramos BP, Paspalas CD, Shu Y, Simen A, Duque A, Vijayraghavan S, Brennan A, Dudley A, Nou E, Mazer JA, McCormick DA, Arnsten AFT (2007) α2A-Adrenoceptors Strengthen Working Memory Networks by Inhibiting cAMP-HCN Channel Signaling in Prefrontal Cortex. Cell 129:397–410.

Whiting MD, Hamm RJ (2006) Traumatic brain injury produces delay-dependent memory impairment in rats. J Neurotrauma 23:1529–1534.

Wilde EA, Newsome MR, Bigler ED, Pertab J, Merkley TL, Hanten G, Scheibel RS, Li X, Chu Z, Yallampalli R, Hunter JV, Levin HS (2011) Brain imaging correlates of verbal working memory in children following traumatic brain injury. International Journal of Psychophysiology 82:86–96.

Wimmer ME, Hernandez PJ, Blackwell J, Abel T (2012) Aging impairs hippocampus-

dependent long-term memory for object location in mice. NBA 33:2220–2224.

Winters BD, Saksida LM, Bussey TJ (2008) Object recognition memory: Neurobiological mechanisms of encoding, consolidation and retrieval. Neuroscience & Biobehavioral Reviews 32:1055–1070.

Witgen BM, Lifshitz J, Smith ML, Schwarzbach E, Liang SL, Grady MS, Cohen AS (2005) Regional hippocampal alteration associated with cognitive deficit following experimental brain injury: A systems, network and cellular evaluation. Neuroscience 133:1–15.

Witt ST, Lovejoy DW, Pearlson GD, Stevens MC (2010) Decreased prefrontal cortex activity in mild traumatic brain injury during performance of an auditory oddball task. Brain Imaging and Behavior 4:232–247.

Yamamoto J, Suh J, Takeuchi D, Tonegawa S (2014) Successful Execution of Working Memory Linked to Synchronized High-Frequency Gamma Oscillations. Cell 157:845–857.

Yizhar O, Fenno LE, Prigge M, Schneider F, Davidson TJ, O'Shea DJ, Sohal VS, Goshen I, Finkelstein J, Paz JT, Stehfest K, Fudim R, Ramakrishnan C, Huguenard JR, Hegemann P, Deisseroth K (2011) Neocortical excitation/inhibition balance in information processing and social dysfunction. Nature 477:171–178.

Yoon T, Okada J, Jung MW, Kim JJ (2008) Prefrontal cortex and hippocampus subserve different components of working memory in rats. Learning & Memory 15:97–105.

Zaloshnja E, Miller T, Langlois JA, Selassie AW (2008) Prevalence of long-term disability

from traumatic brain injury in the civilian population of the United States, 2005. J Head Trauma Rehabil 23:394–400.